PHASES OF QCD

THOMAS SCHÄFER
Department of Physics
North Carolina State University
Raleigh, NC 27695

In these lectures we provide an introduction to the phase structure of QCD. We begin with a brief discussion of QCD, the symmetries of QCD, and what we mean by a "phase of QCD". In the main part of the lectures we discuss the phase diagram of QCD as a function of the temperature and the baryon density. We focus, in particular, on the high temperature plasma phase, the low temperature and low density nuclear phase, and the high density color superconducting phases.

1. Introduction

In these lectures we wish to provide an introduction to the phase structure of QCD. The phase of QCD that we live in is characterized by the permanent confinement of quarks, and the existence of a large mass gap. There are several reasons for trying to understand whether other phases of QCD exist, and what conditions are required in order to observe these phases:

1) Other phases of QCD exist in the universe: The universe started out in a hot and dense phase. It expanded and cooled and about 10^{-5} sec after the big bang it passed through a transition from a quark gluon plasma to a hadronic phase. Even today, extreme conditions exist in the universe. In supernova explosions matter is heated to several tens of MeV, sufficient to evaporate ordinary nuclei. The compact remnants have central densities several times larger than the saturation density of nuclear matter.

2) Exploring the entire phase diagram help us to understand the phase that we live in: The structure of hadrons and their interactions are determined by the symmetries of the QCD vacuum. Studying the phase diagram of QCD allows us to understand the possible ways in which the symmetries of QCD can be realized.

3) QCD simplifies in extreme environments: At scales relevant to hadrons QCD is strongly coupled and we have to rely on numerical simulations in order to test predictions of QCD. In the case of large tempera-

ture or large baryon density there is a large external scale in the problem. Asymptotic freedom implies that the bulk of the system is governed by weak coupling. As a result, we can study QCD matter in a regime where quarks and gluons are indeed the correct degrees of freedom.

In these lectures we will give a general introduction into the physics of the QCD phase diagram. There are several excellent text books and reviews articles that provide a much more detailed discussion of QCD and hadronic matter at finite temperature and density [1,2,3]. We also recommend more specialized texts on field theory at finite temperature [4,5,6] and density [7,8], as well as reviews on the phase structure of dense matter [9,10,11] and on color superconductivity [12,13,14,15]. In this write-up we will not try to give a summary of the experimental program at RHIC and the SPS. A useful reference is the series of white papers that was recently published by the RHIC collaborations [16]. We will also not review implications of the phase structure of QCD for the structure of compact stars or observational constraints on the behavior of dense matter [10,17,18].

2. QCD and symmetries

2.1. *Introduction*

We begin with a brief review of QCD and the symmetries of QCD. The elementary degrees of freedom are quark fields $\psi^a_{\alpha,f}$ and gluons A^a_μ. Here, a is color index that transforms in the fundamental representation for fermions and in the adjoint representation for gluons. Also, f labels the quark flavors u, d, s, c, b, t. In practice, we will focus on the three light flavors up, down and strange. The QCD lagrangian is

$$\mathcal{L} = \sum_f^{N_f} \bar{\psi}_f (i\not{D} - m_f)\psi_f - \frac{1}{4} G^a_{\mu\nu} G^a_{\mu\nu}, \tag{1}$$

where the field strength tensor is defined by

$$G^a_{\mu\nu} = \partial_\mu A^a_\nu - \partial_\nu A^a_\mu + g f^{abc} A^b_\mu A^c_\nu, \tag{2}$$

and the covariant derivative acting on quark fields is

$$i\not{D}\psi = \gamma^\mu \left(i\partial_\mu + g A^a_\mu \frac{\lambda^a}{2} \right) \psi. \tag{3}$$

QCD has a number of interesting properties. Most remarkably, even though QCD accounts for the rich phenomenology of hadronic and nuclear physics, it is an essentially parameter free theory. As a first approximation, the

masses of the light quarks u, d, s are too small to be important, while the masses of the heavy quarks c, b, t are too heavy. If we set the masses of the light quarks to zero and take the masses of the heavy quarks to be infinite then the only parameter in the QCD lagrangian is the coupling constant, g. Once quantum corrections are taken into account g becomes a function of the scale at which it is measured. Gross, Wilczek and Politzer showed that [19,20]

$$g^2(q^2) = \frac{16\pi^2}{b\log(q^2/\Lambda^2_{QCD})}, \quad b = \frac{11N_c}{3} - \frac{2N_f}{3}. \tag{4}$$

If the scale q^2 is large then the coupling is small, but in the infrared the coupling becomes large. This is the famous phenomenon of asymptotic freedom. Since the coupling depends on the scale the dimensionless parameter g is traded for a dimensionful scale parameter Λ_{QCD}. In essence, Λ_{QCD} is the scale at which the theory becomes non-perturbative.

Since Λ_{QCD} is the only dimensionful quantity in QCD ($m_q = 0$) it is not really a parameter of QCD, but reflects our choice of units. In standard units, $\Lambda_{QCD} \simeq 200\,\mathrm{MeV} \simeq 1\,\mathrm{fm}^{-1}$. Note that hadrons indeed have sizes $r \sim \Lambda^{-1}_{QCD}$.

Another important feature of the QCD lagrangian are its symmetries. First of all, the lagrangian is invariant under local gauge transformations $U(x) \in SU(3)_c$

$$\psi(x) \to U(x)\psi(x), \qquad A_\mu(x) \to U(x)A_\mu U^\dagger(x) + iU(x)\partial_\mu U^\dagger(x), \tag{5}$$

where $A_\mu = A^a_\mu(\lambda^a/2)$. While the gauge symmetry is intimately connected with the dynamics of QCD we observe that the interactions are completely independent of flavor. If the masses of the quarks are equal, $m_u = m_d = m_s$, then the theory is invariant under arbitrary flavor rotations of the quark fields

$$\psi_f \to V_{fg}\psi_g, \tag{6}$$

where $V \in SU(3)$. This is the well known flavor (isospin) symmetry of the strong interactions. If the quark masses are not just equal, but equal to zero, then the flavor symmetry is enlarged. This can be seen by defining left and right-handed fields

$$\psi_{L,R} = \frac{1}{2}(1 \pm \gamma_5)\psi. \tag{7}$$

In terms of L/R fields the fermionic lagrangian is

$$\mathcal{L} = \bar\psi_L(i\not{D})\psi_L + \bar\psi_R(i\not{D})\psi_R + \bar\psi_L M\psi_R + \bar\psi_R M\psi_L, \tag{8}$$

where $M = \mathrm{diag}(m_u, m_d, m_s)$. We observe that if quarks are massless, $m_u = m_d = m_s = 0$, then there is no coupling between left and right handed fields. As a consequence, the lagrangian is invariant under independent flavor transformations of the left and right handed fields.

$$\psi_{L,f} \to L_{fg}\psi_{L,g}, \qquad \psi_{R,f} \to R_{fg}\psi_{R,g}, \tag{9}$$

where $(L, R) \in SU(3)_L \times SU(3)_R$. In the real world, of course, the masses of the up, down and strange quarks are not zero. Nevertheless, since $m_u, m_d \ll m_s < \Lambda_{QCD}$ QCD has an approximate chiral symmetry.

Finally, we observe that the QCD lagrangian has two $U(1)$ symmetries,

$$U(1)_B : \qquad \psi_L \to e^{i\phi}\psi_L, \qquad \psi_R \to e^{i\phi}\psi_R, \tag{10}$$

$$U(1)_A : \qquad \psi_L \to e^{i\alpha}\psi_L, \qquad \psi_R \to e^{-i\alpha}\psi_R. \tag{11}$$

The $U(1)_B$ symmetry is exact even if the quarks are not massless. The axial $U(1)_A$ symmetry is exact at the classical level but it is broken in the quantum theory. This phenomenon is referred to as an anomaly. The divergence of the $U(1)_A$ current is given by

$$\partial^\mu j^5_\mu = \frac{N_f g^2}{16\pi^2} G^a_{\mu\nu}\tilde{G}^a_{\mu\nu}, \tag{12}$$

where $\tilde{G}^a_{\mu\nu} = \epsilon_{\mu\nu\alpha\beta}G^a_{\alpha\beta}/2$ is the dual field strength tensor.

2.2. *Phases of QCD*

The phases of QCD are related to the different ways in which the symmetries of QCD can be realized in nature. We first consider the local gauge symmetry. There are three possible realizations of a local symmetry:

1) Coulomb Phase: In a Coulomb phase the gauge symmetry is unbroken, the gauge bosons are massless and mediate long range forces. In particular, the potential between two heavy charges is a Coulomb potential, $V(r) \sim 1/r$.

2) Higgs Phase: In a Higgs phase the gauge symmetry is spontaneously broken and the gauge bosons acquire a mass. As a consequence, the potential between two heavy charges is a Yukawa potential, $V(r) \sim \exp(-mr)/r$. We should note that local gauge symmetry is related to the fact that we are using redundant variables (the four-component vector potential A_μ describes the two polarization states of a massless vector boson), and that therefore a local symmetry cannot really be broken (Elitzur's theorem [21]). We will discuss the exact meaning of "spontaneous gauge symmetry breaking" in Sect. 4.6 below.

3) Confinement: In a confined phase all the physical excitations are singlets under the gauge group. Confinement can be strictly defined only in theories that do not have light fields in the fundamental representation. In that case, confinement implies that the potential between two heavy charges rises linearly, $V(r) \sim kr$. This is called a string potential. If there are light fields in the fundamental representation, as in QCD with light quarks, then the string can break and the potential levels off.

It is interesting to note that all three realizations of gauge symmetry play a role in the standard model. The $U(1)$ of electromagnetism is in a Coulomb phase, the $SU(2)$ is realized in a Higgs phase, and the $SU(3)$ of color is confined. Also, as we shall see in these lectures, there are phases of QCD in which the color symmetry is not confined but realized in a Higgs or Coulomb phase.

Different phases of matter, like liquid vs solid, superfluid vs normal, are related to the realization of global symmetries. In QCD at zero baryon density spacetime symmetries as well as $U(1)$ symmetries cannot be broken [22,23]. This means that phases of QCD matter are governed by the realization of the chiral $SU(3)_L \times SU(3)_R$ symmetry. If the baryon density is not zero both space-time and $U(1)$ symmetries can break and the phase diagram is much richer.

2.3. *The QCD vacuum*

In the QCD ground state at zero temperature and density chiral symmetry is spontaneously broken by a quark-anti-quark condensate $\langle\bar{\psi}\psi\rangle$. We can view the chiral condensate as a matrix in flavor space. In the QCD vacuum

$$\langle\bar{\psi}^f_L\psi^g_R\rangle = \langle\bar{\psi}^f_R\psi^g_L\rangle \simeq -\delta^{fg}(230\,\mathrm{MeV})^3, \tag{13}$$

which implies that chiral symmetry is spontaneously broken according to $SU(3)_L \times SU(3)_R \to SU(3)_V$. The $SU(3)_V$ flavor symmetry is broken explicitly by the difference between the masses of the up, down and strange quark. Since $m_s \gg m_u, m_d$ the $SU(2)$ isospin symmetry is a much better symmetry than $SU(3)$ flavor symmetry.

Chiral symmetry breaking has important consequences for the dynamics of QCD at low energy. Goldstone's theorem implies that the breaking of $SU(3)_L \times SU(3)_R \to SU(3)_V$ is associated with the appearance of an octet of (approximately) massless pseudoscalar Goldstone bosons. Chiral symmetry places important restrictions on the interaction of the Goldstone

bosons. These constraints are most easily obtained from the low energy effective chiral lagrangian. The transformations properties of the chiral field Σ follow from the structure of the chiral order parameter,

$$\Sigma \to L\Sigma R^\dagger, \qquad \Sigma^\dagger \to R\Sigma^\dagger L^\dagger, \tag{14}$$

for $(L,R) \in SU(3)_L \times SU(3)_R$. In the vacuum we can take $\langle\Sigma\rangle = 1$. Goldstone modes are fluctuations of the order parameter in the coset space $SU(3)_L \times SU(3)_R/SU(3)_V$. They are parameterized by unitary matrices $\Sigma = \exp(i\lambda^a\phi^a/f_\pi)$ where λ^a are the Gell-Mann matrices and $f_\pi = 93$ MeV is the pion decay constant. At low energy the effective lagrangian for Σ can be organized as an expansion in the number of derivatives. At leading order in (∂/f_π) there is only one structure which is consistent with chiral symmetry, Lorentz invariance and C,P,T. This is the lagrangian of the non-linear sigma model

$$\mathcal{L} = \frac{f_\pi^2}{4}\mathrm{Tr}\left[\partial_\mu\Sigma\partial^\mu\Sigma^\dagger\right] + \ldots. \tag{15}$$

In order to show that the parameter f_π is related to the pion decay amplitude we have to gauge the non-linear sigma model. This is achieved by introducing the gauge covariant derivative $\nabla_\mu\Sigma = \partial_\mu\Sigma + ig_w W_\mu\Sigma$ where W_μ is the charged weak gauge boson and g_w is the weak coupling constant. The gauged non-linear sigma model gives a pion-W boson interaction $\mathcal{L} = g_w f_\pi W_\mu^\pm \partial^\mu\pi^\mp$ which agrees with the standard definition of f_π in terms of the pion-weak axial current matrix element.

Expanding Σ in powers of the pion, kaon and eta fields ϕ^a we can derive low energy predictions for Goldstone boson scattering. In the pion sector we have

$$\mathcal{L} = \frac{1}{2}(\partial_\mu\phi^a)^2 + \frac{1}{6f_\pi^2}\left[(\phi^a\partial_\mu\phi^a)^2 - (\phi^a)^2(\partial_\mu\phi^b)^2\right] + O\left(\frac{\partial^4}{f_\pi^4}\right), \tag{16}$$

which shows that the low energy $\pi\pi$-scattering amplitude is completely determined by f_π. Higher order corrections originate from loops and higher order terms in the effective lagrangian.

In QCD chiral symmetry is explicitly broken by the quark mass term $\bar\psi M\psi$, where $M = \mathrm{diag}(m_u, m_d, m_s)$ is the quark mass matrix. In order to determine how the quark masses appear in the effective lagrangian it is useful to promote the mass matrix to a field which transforms as $M \to LMR^\dagger$ under chiral transformations. This means that the mass term is chirally invariant and explicit breaking only appears when M is replaced by its vacuum value. There is a unique term in the chiral lagrangian which

is $SU(3)_L \times SU(3)_R$ invariant and linear in M. To order $O(\partial^2, M)$ the effective lagrangian is

$$\mathcal{L} = \frac{f_\pi^2}{4}\mathrm{Tr}\left[\partial_\mu \Sigma \partial^\mu \Sigma^\dagger\right] + \left[B\mathrm{Tr}(M\Sigma^\dagger) + h.c.\right] + \ldots . \tag{17}$$

The mass term acts a potential for the chiral field. We observe that if the quark masses are real and positive then the minimum of the potential is at $\langle\Sigma\rangle = 1$, as expected. If some of the quark masses are negative unusual phases of QCD can appear, see [24].

The vacuum energy is $E_{vac} = -2B\mathrm{Tr}[M]$. Using $\langle\bar{\psi}\psi\rangle = \partial E_{vac}/(\partial m)$ we find $\langle\bar{\psi}\psi\rangle = -2B$. Fluctuations around the vacuum value $\Sigma = 1$ determine the Goldstone boson masses. The pion mass satisfies the Gell-Mann-Oaks-Renner relation

$$m_\pi^2 f_\pi^2 = (m_u + m_d)\langle\bar{\psi}\psi\rangle \tag{18}$$

and analogous relations exist for the kaon and eta masses.

2.4. *QCD vacuum for different N_c and N_f*

QCD is a strongly interacting gauge theory with almost massless quarks. It seems natural that in such a theory bound states of quarks and antiquarks are formed, that bound states in the scalar channel condense, and that chiral symmetry is broken. But even if chiral symmetry breaking is not surprising, it is not a priori clear whether the observed pattern of chiral symmetry breaking and confinement is required on general grounds, or whether it is a particular dynamical feature of QCD. Some obvious questions are: Are all asymptotically free gauge theories confining? Does confinement imply chiral symmetry breaking (or vice versa)? Is the symmetry breaking pattern $SU(3)_L \times SU(3)_R \to SU(3)_V$ unique?

An interesting context in which these questions can be studied is the phase diagram of QCD and supersymmetric generalizations of QCD as a function of N_c and N_f, see Fig. 1. For our purposes supersymmetric QCD is simply a QCD-like theory with extra fermions in the adjoint representation and extra colored scalar fields. Including supersymmetric theories is useful because supersymmetry provides additional constraints that determine the symmetries of the ground state. The following interesting results have been obtained:

1) In supersymmetric QCD there is a window $N_c + 1 < N_f < 3N_c$ in which the theory is asymptotically free but not confining [25]. There are several reasons to believe that such a window exists in QCD, too. One is

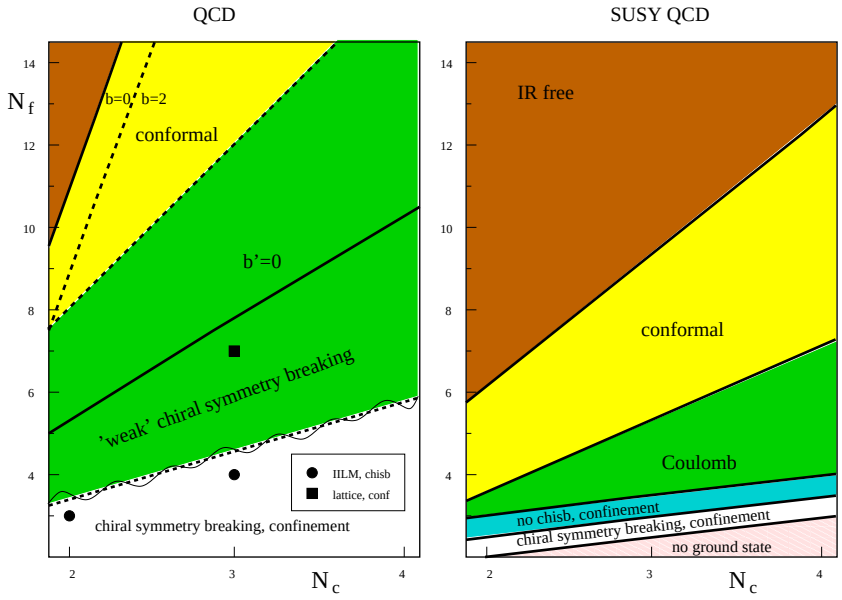

Figure 1. Ground state of QCD and SUSY QCD as a function of N_c and N_f. The symmetry breaking pattern in SUSY QCD was clarified in a series of papers by Seiberg and collaborators. The phase structure of QCD is an educated guess, discussed in more detail in the review (Schäfer and Shuryak, 1998).

.

the fact that as a function of the number of flavors the second coefficient of the beta function changes sign before the first one does [26]. In this regime the coupling constant flows to a finite value at large distance and the theory is scale invariant.

2) Supersymmetric QCD also provides examples for theories that have confinement but no chiral symmetry breaking. This happens for $N_f = N_c + 1$. This theory contains both massless mesons and massless baryons. An important constraint is provided by the 't Hooft anomaly matching conditions [27,28]. In QCD these relations show that confinement without chiral symmetry breaking is a possibility for $N_f = 2$, but ruled out for $N_f > 2$.

3) The 't Hooft consistency conditions also provide constraints on the symmetry breaking pattern. In QCD these conditions are not sufficiently strong to fix the ground state completely, but one can show that $SU(3)_L \times SU(3)_R \to SU(3)_V$ is favored in the limit $N_c \to \infty$ [29].

4) One can show that in QCD chiral symmetry breaking implies a non-zero quark condensate [30]. In particular, one can rule out the possibility that $\langle\bar{\psi}\psi\rangle = 0$, but $\langle(\bar{\psi}\psi)^2\rangle \neq 0$.

3. QCD at finite Temperature

3.1. *General Arguments*

In this section we shall discuss the phase structure of QCD at non-zero temperature. We begin by reviewing some general arguments in favor of the existence of a critical temperature T_c above which quarks and gluons are deconfined and chiral symmetry is restored.

Asymptotic freedom clearly suggests that the high temperature phase is a weakly interacting plasma [31,32]. Consider a non-interacting gas of quarks and gluons at high temperature. The typical momenta are on the order of the temperature, $p \sim 3T$, and the density is $n \sim T^3$. Now imagine that we turn on the coupling. Does this lead to a qualitative change in the system? Quarks and gluon can scatter but since the typical momenta are large a significant change in the momentum of the scattered particles requires a large momentum transfer. Asymptotic freedom implies that the effective coupling at this scale is small, and that large angle scattering events are rare. If the change of momentum is small then the scattering involves large distances and the interaction is modified by the dense medium. We will see below that the quark-gluon medium screens the interaction and that the effective interaction is again weak. There is a small subtlety here, as static magnetic interactions are not screened. This implies that high temperature QCD has a genuinely non-perturbative sector, but this sector is not important as far as bulk properties of the high temperature phase are concerned. We conclude that the assumption of a weakly interacting quark-gluon system at high temperature leads to a self consistent picture. Since this system will exhibit medium effects, such as damping and screening, collective modes, etc. that are typical of plasmas it was termed the quark gluon plasma (QGP) [32,33].

It is instructive to consider a simple model of the equation of state. The pressure and energy density of non-interacting massless particles is

$$P = \epsilon/3, \qquad \epsilon = g\frac{\pi^2}{30}T^4 \begin{cases} 1 & \text{bosons} \\ 7/8 & \text{fermions} \end{cases}, \tag{19}$$

where g is the number of degrees of freedoms. In a quark gluon plasma we have $g_q = 4N_f N_c$ quarks and $g_g = 2(N_c^2 - 1)$ gluon degrees of freedom. For

$N_f = 2$ we get $g_{eff} = g_g + 7g_q/8 = 37$ and

$$P = \frac{37\pi^2}{90}T^4. \tag{20}$$

At low temperature the relevant degrees are Goldstone bosons. Near T_c we can assume that Goldstone bosons are approximately massless and the number of degrees of freedom is $g = (N_f^2 - 1)$. For $N_f = 2$ we get $g = 3$ and

$$P = \frac{3\pi^2}{90}T^4. \tag{21}$$

This result seems to show that the pressure in the low temperature phase is always smaller than the pressure in the high temperature phase. This cannot be right as it would imply that the phase with chiral symmetry breaking is never favored. The problem is that there are non-perturbative effects in the low temperature phase. These effects give rise to a negative vacuum energy and a positive vacuum pressure. Lorentz invariance implies that the vacuum energy momentum tensor is of the form $T_{\mu\nu} = Bg_{\mu\nu}$ and

$$\epsilon_{vac} = -P_{vac} = +B. \tag{22}$$

In QCD the vacuum energy satisfies the trace anomaly relation

$$\epsilon_{vac} = -\frac{b}{32}\langle\frac{\alpha}{\pi}G^2\rangle \simeq -0.5 \text{ GeV/fm}^3. \tag{23}$$

The numerical value comes from QCD sum rule determinations of the gluon condensate [34] $\langle\alpha G^2\rangle$ and has a considerable uncertainty. We can now obtain an estimate of the transition temperature by requiring that the pressure in the low temperature phase equals the pressure in the quark gluon phase. We find

$$T_c = \left(\frac{45B}{17\pi^2}\right)^{1/4} \simeq 180 \text{ MeV} \tag{24}$$

We can also determine the critical energy density. The energy densities just below and just above the critical temperature are given by

$$\epsilon(T_c^-) = \frac{3\pi^2}{30}T_c^4 \simeq 130 \text{ MeV/fm}^3, \tag{25}$$

$$\epsilon(T_c^+) = \frac{37\pi^2}{30}T_c^4 + B \simeq 2000 \text{ MeV/fm}^3. \tag{26}$$

We observe that the energy density in the QGP exceeds 1 GeV/fm^3. This should be compared to the energy density in cold nuclear matter which is about 150 MeV/fm^3.

An independent estimate of the transition temperature can be obtained using the chiral effective theory. We saw that the chiral condensate is related to the mass dependence of the vacuum energy. At tree level and to leading order in the quark masses the condensate is given by the coefficient B in the chiral lagrangian. We can also calculate corrections to this result due to thermal Goldstone boson fluctuations. At leading order it is sufficient to consider the free energy of a non-interacting pion gas

$$F = (N_f^2 - 1)T \int \frac{d^3p}{(2\pi)^3} \log\left(1 - e^{-E_\pi/T}\right), \tag{27}$$

where $E_\pi = \sqrt{p^2 + m_\pi^2}$. The quark condensate is $\langle\bar{\psi}\psi\rangle = (N_f)^{-1}\partial F/\partial m$. Equation (27) depends on the quark mass only through the pion mass. Using the Gell-Mann-Oakes-Renner relation (18) we find [35]

$$\langle\bar{\psi}\psi\rangle_T = \langle\bar{\psi}\psi\rangle_0 \left\{1 - \frac{N_f^2 - 1}{3N_f}\left(\frac{T^2}{4f_\pi^2}\right) + \ldots\right\}. \tag{28}$$

This result indicates that the chiral condensate vanishes at a critical temperature

$$T_c \simeq 2f_\pi\sqrt{\frac{3N_f}{N_f^2 - 1}} \simeq 200\,\mathrm{MeV} \quad (N_f = 3), \tag{29}$$

which is roughly consistent with the estimate obtained in equ. (24).

3.2. *Chiral Symmetry Restoration*

In the vicinity of the phase transition QCD is genuinely non-perturbative and it is hard to improve on the rough estimates provided in the previous section. One possibility for determining the transition temperature and elucidating the nature of the phase transition is the use of large scale numerical simulations. We will discuss this approach in Sect. 3.4. Before we do so we would like to review certain general statements about the phase transition that follow from the symmetries of the low and high temperature phase.

We begin with the chiral phase transition. We shall assume that the chiral transition is a second order phase transition, i.e. the order parameter goes to zero continuously. We will explore the consequences of this assumption and check whether it leads to a consistent picture. In the vicinity of a second order phase transition the order parameter fluctuates on all length scales and the correlation length diverges. This means that the

Table 1. Correspondence between the chiral phase transition in QCD and the ferromagnetic transition in a four-component magnet.

$SU(2)_L \times SU(2)_R$	QCD	$O(4)$	magnet
$\langle\bar{\psi}\psi\rangle$	χ condensate	$\vec{M}$	magnetization
m_q	quark mass	H_3	magnetic field
$\vec{\pi}$	pions	$\vec{\phi}$	spin waves

details of the interaction are not important, and only the symmetry of the order parameter matters.

In QCD with two flavors the order parameter is a 2×2 matrix $U^{fg} = \langle\bar{\psi}_L^f \psi_R^g\rangle$. We can define a four component vector ϕ^a by $U^{fg} = \phi^a (\tau^a)^{fg}$ with $\tau^a = (\vec{\tau}, 1)$. Chiral transformations $(L, R) \in SU(3)_L \times SU(3)_R$ correspond to rotations $\phi^a \to R^{ab}\phi^b$ with $R \in SO(4)$. In the low temperature phase chiral symmetry is broken and $\langle\phi^a\rangle = \sigma\delta^{a0}$. Near T_c the order parameter is small and we we can expand the free energy in powers of the order parameter and its derivatives. Chiral symmetry implies that only the length of ϕ^a can enter. To order ϕ^4 and to leading order in gradients of the fields we have

$$F = \int d^3x \left\{ \frac{1}{2}(\vec{\nabla}\phi^a)^2 + \frac{\mu^2}{2}(\phi^a\phi^a) + \frac{\lambda}{4}(\phi^a\phi^a)^2 + \ldots \right\}, \qquad (30)$$

where μ^2, λ are parameters that depend on the temperature. Equ. (30) is the Landau-Ginzburg effective action. Note that fluctuations of the order parameter are dominated by static fields $\phi^a(\vec{x}, t) = \phi^a(\vec{x})$. This will be explained in more detail in Sect. 3.5. The main observation is that fluctuations with energy much smaller than πT are described by a three dimensional theory.

Stability requires that $\lambda > 0$. Below the critical temperature $\mu^2 < 0$ and chiral symmetry is broken. At T_c the parameter μ^2 changes sign and we can write $\mu^2 = \mu_0^2 t$ where $t = (T - T_c)/T_c$ is the reduced temperature. As a first approximation we can ignore fluctuations and study the Landau-Ginzburg action in the mean field approximation. In that case the chiral order parameter goes to zero as $\langle\phi^0\rangle \sim t^{1/2}$. This result is modified if fluctuations are included. This can be done using renormalization group methods or numerical simulations. These methods also demonstrate that near T_c higher order operators not included in equ. (30) are indeed irrelevant. The results are

$$\begin{aligned} C &\sim t^{-\alpha} && \alpha = -0.19, \\ \langle\bar{\psi}\psi\rangle &\sim t^{\beta} && \beta = 0.38, \\ m_\pi &\sim t^{\nu} && \nu = 0.73, \end{aligned} \qquad (31)$$

where C is the specific heat and the Goldstone boson mass m_π is defined as the inverse correlation length of spatial fluctuations of the pion field.

The coefficients α, β, ν are called the critical indices of the phase transition. These coefficients are universal, i.e. independent of the details of the microscopic details. For example, the critical indices of the chiral phase transition in QCD agree with the critical indices of a four-component magnet in $d = 3$ space dimensions, see Table 1.

In QCD with $N_f = 3$ flavors the order parameter is a 3×3 matrix U^{fg}. The main new ingredient in the Landau-Ginzburg theory is a chirally invariant cubic term $\det(U) + \text{h.c.}$ It is easy to check that the cubic term will lead to an effective potential that has two degenerate minima at the transition temperature. This implies that the transition is first order and the order parameter goes to zero discontinuously. Even if the coefficient of the cubic term is zero initially, fluctuations tend to generate a cubic interaction as $T \to T_c$. A transition of this type is called fluctuation induced first order.

3.3. *Deconfinement*

It is not immediately obvious how to identify the symmetry associated with the deconfinement transition. In order to make contact with the lattice formulation discussed in Sect. 3.4 we will study this question in euclidean space, i. e. with the time variable analytically continued to imaginary time, $t \to it$. We first derive an expression for the potential between two heavy quarks. Consider the Dirac equation for a massive quark in a gluon background field

$$\left(\partial_0 - igA_0 - \vec{\alpha}(i\vec{\nabla} + g\vec{A}) + \gamma_0 M\right)\psi = 0. \tag{32}$$

In the limit $m_Q \to \infty$ we can ignore the spatial components of the covariant derivative. The quark propagator is

$$S(x, x') \simeq \exp\left(ig\int A_0 dt\right)\left(\frac{1+\gamma_0}{2}\right)e^{-m(t-t')}\delta(\vec{x} - \vec{x}'). \tag{33}$$

The heavy quark potential is related to the amplitude for creating a heavy quark-anti-quark pair at time $t = 0$, separating the pair by a distance R, and finally annihilating the two quarks at time $t = T$. The amplitude is related to the Wilson loop

$$W(R, T) = \exp\left(ig\oint A_\mu dz_\mu\right), \tag{34}$$

where the integration contour is a $R \times T$ rectangle and we have dropped the Dirac projection operators $(1+\gamma_0)/2$. If $T \gg R$ the amplitude is dominated by the ground state and we expect $W(R,T) \sim \exp(-V(R)T)$ where $V(R)$ is the heavy quark potential. Confinement implies that $V(R) \sim kR$ and the Wilson loop satisfies an area law

$$W(R,T) \sim \exp(-kA),. \tag{35}$$

where $A = RT$. In order to construct a local order parameter we consider the Polyakov line

$$P(\vec{x}) = \frac{1}{N_c}\mathrm{Tr}[L(\vec{x})] = \frac{1}{N_c}P\mathrm{Tr}\left[\exp\left(ig\int_0^\beta A_0 dt\right)\right]. \tag{36}$$

As we will explain in more detail in the next section gauge fields are periodic in imaginary time with period $\beta = 1/T$. The Polyakov line can be interpreted as the free energy of a single quark, $\langle P\rangle \sim \exp(-m_Q\beta)$. In the confined phase we expect that the energy of an isolated quark is infinite, while in the deconfined phase it is finite. This implies that

$$\langle P\rangle = 0 \quad \text{confined,} \qquad \langle P\rangle \neq 0 \quad \text{deconfined.} \tag{37}$$

The global symmetry of the order parameter is [36] $P \to zP$ with $z = \exp(2\pi ki/N_c) \in Z_{N_c}$. Since Z_{N_c} is the center of the gauge group $SU(N_c)$ this is sometimes called the center symmetry. Color singlet correlation functions always involve combinations of Polyakov lines that are invariant under center transformations. A heavy baryon correlation function, for example, is of the form $\mathrm{tr}[(L(\vec{x}))^{N_c}]$ and is invariant because $z^{N_c} = 1$. A non-zero expectation value for the Polyakov line, on the other hand, breaks center symmetry.

Note that the symmetry is broken in the high temperature phase and restored in the low temperature phase. This might seem somewhat unusual, but there are examples of spin systems that have an equivalent "dual" description in terms of a gauge theory [37]. In the dual theory the high and low temperature phases are interchanged.

The Z_{N_c} Landau-Ginzburg action is given by [38]

$$F = \int d^3x \left\{\frac{1}{2}|\vec{\nabla}P|^2 + \mu^2|P|^2 + g\mathrm{Re}(P^3) + \lambda|P|^4 + \ldots\right\}. \tag{38}$$

The cubic term is allowed only if $N_c = 3$. As in the case of the chiral phase transition we expect the cubic term to drive the transition first order. The two color theory is in the equivalence class of the Z_2 Ising model, which is known to have a second order transition. The three color theory is in the

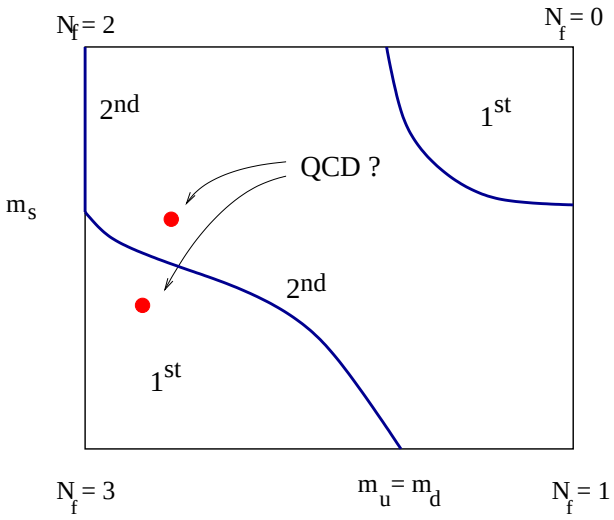

Figure 2. Phase diagram of QCD in the $m - m_s$ mass plane. The plot shows the universality class of the chiral/deconfinement transition for different values of m, m_s.

equivalence class of a three state Potts model, which does indeed show a first order transition.

The phase structure as a function of the light quark mass $m = m_u = m_d$ and the strange quark mass m_s is summarized in Fig. 2. The lower left hand corner of the diagram is $m = m_s = 0$ and corresponds to three massless quarks. In that case we expect a first order chiral phase transition. Along the diagonal we have $m = m_s$ and the $SU(3)_V$ flavor symmetry is exact. As the quark masses increase the strength of the first order transition becomes weaker and the transition eventually ends at a second order critical point. If the light quarks are kept massless as the strange quark mass is increased the endpoint of the first order transition is a tricritical point at which the the endpoint of the first order transition in the three flavor theory meets the second order transition of the two flavor theory. This transition turns into a smooth crossover as soon as the light quarks are given a small mass.

The upper right hand corner of the plot is $m = m_s \to \infty$ and corresponds to the pure glue theory which has a first order transition. Dynamical quarks break the Z_{N_c} symmetry and the strength of the first order transition decreases as the quark masses are lowered. The first order transition in the pure glue theory ends on a line of second order transitions.

We do not know with certainty where the physical point is located on

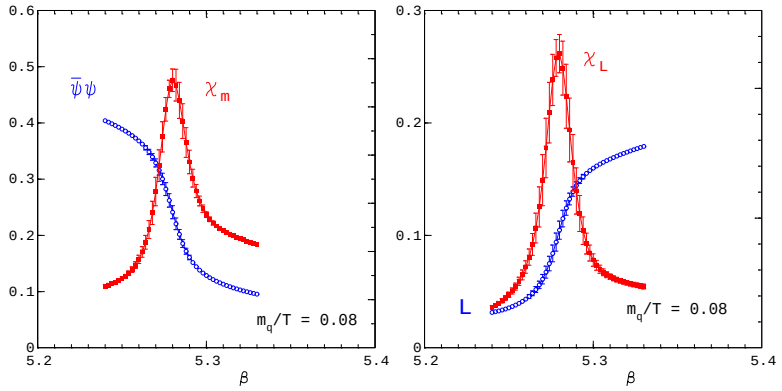

Figure 3. Chiral and deconfinement transitions for $N_f = 2$ dynamical quark flavors, from (Karsch 2002). The two figure show the chiral condensate and the Polyakov line as a function of the bare coupling $\beta = 6/g^2$ (In this figure, β is not $1/T$). Asymptotic freedom implies that on a fixed lattice $N_\tau \times N_\sigma^3$ increasing β corresponds to increasing the temperature. The susceptibilities χ_m, χ_L are related to order parameter fluctuations, e.g. $\chi_L = n_\sigma^3(\langle L^2\rangle - \langle L\rangle^2)$.

this phase diagram. Lattice calculations currently favor the possibility that the phase transition is in the crossover region, closer to the first order chiral transition than to the first order deconfinement transition.

We should emphasize that Fig. 2 focuses on regions of the phase diagram in which there is a sharp phase transition and the order parameter is a non-analytic function at T_c. The figure should not be taken to imply that the chiral and deconfinement transitions are completely separate phenomena, or that the transition cannot be observed in the crossover region. Fig. 3 shows the order parameter as well as the order parameter susceptibilities for the chiral and deconfinement transitions. The results were obtained from lattice calculations with semi-realistic values of the quark masses. We observe that even though both transitions are crossovers clear peaks in the susceptibilities are still visible. We also note that the chiral and deconfinement transitions occur at the same temperature. This can be understood in models that include a non-zero coupling between the effective actions for the chiral and deconfinement order parameters [39,40,41].

3.4. *Lattice QCD*

Symmetry arguments cannot determine the critical temperature, the critical energy density, and many other properties of matter near the phase

transition. In order to compute these properties we have to rely on numerical simulations of the QCD partition function

$$Z = \mathrm{Tr}[e^{-\beta H}], \;\; \beta = 1/T \qquad F = TV{-}1 \log(Z), \tag{39}$$

where H is the QCD Hamiltonian, β is the inverse temperature and F is the free energy. We can write the partition function as a quantum mechanical evolution operator $Z = \mathrm{Tr}[e^{-i(-i\beta)H}]$ with imaginary time $\tau = -i\beta$. The evolution operator can be written as a path integral

$$Z = \int dA_\mu d\psi d\bar{\psi} \exp\left(- \int_0^\beta d\tau \int d^3x \; \mathcal{L}_E \right), \tag{40}$$

where $\mathcal{L}_E$ is the imaginary time (euclidean) lagrangian and we have to impose (anti)periodic boundary conditions on the quark and gluon fields

$$A_\mu(\vec{x}, \beta) = A_\mu(\vec{x}, 0), \quad \psi(\vec{x}, \beta) = -\psi(\vec{x}, 0). \tag{41}$$

The path integral is an infinite dimensional integral. In order to perform numerical simulations we have to discretize space and time and introduce a $N_\tau \times N_\sigma^3$ lattice with lattice spacing a. In order to maintain exact gauge invariance on a discrete lattice the gauge fields are discretized in terms of the link variables

$$U_\mu(n) = \exp(igaA_\mu(n)), \tag{42}$$

where $n = (n_\tau, n_x, n_y, n_z)$ labels lattice sites and $\mu = 1, \ldots, 4$. In terms of the link variables it is easy to define a gauge covariant discrete derivative

$$D_\mu \phi \to \frac{1}{a}[U_{-\mu}(n)\phi(n+\mu) - \phi(n)], \tag{43}$$

where $n + \mu$ is the lattice site reached by starting at n and doing one hop in the μ direction. $\phi(n)$ is a scalar field in the fundamental representation. The action of the pure gauge theory is given by

$$S = \frac{2}{g^2} \sum_{n,\mu} \mathrm{Re\ Tr}\left[1 - U_\mu(n) U_\nu(n+\mu) U_{-\mu}(n+\mu+\nu) U_{-\nu}(n+\nu)\right], \tag{44}$$

which involves a loop of link variables called a plaquette. It is easy to check that equ. (44) reduces to the continuum action as $a \to 0$. Fermion fields $\psi(n)$ are discretized on lattice sites. There are some subtleties in discretizing chiral fermions which we do not discuss here [42]. The action is bilinear in the fermion fields. This means that the integral over the fermion fields can be done exactly and we are left with the determinant of a matrix

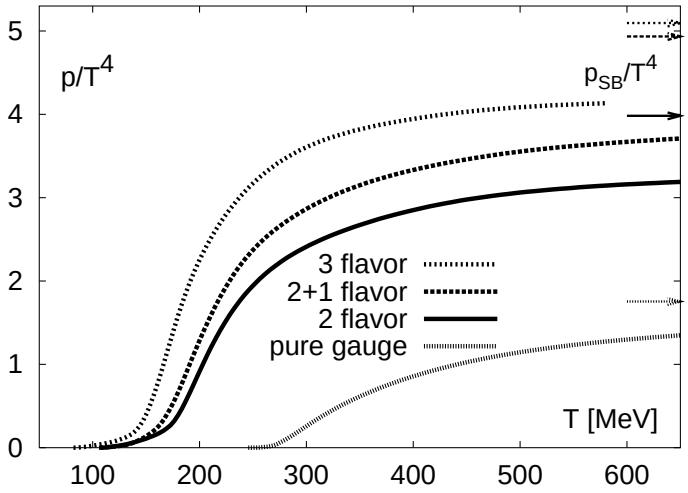

Figure 4. Equation of state obtained in lattice calculations with $N_f = 0, 2, 2+1, 3$ flavors, from Karsch (2002). The 2+1 curve refers to two light flavors and one intermediate mass flavor. The pressure is given in units of T^4. The arrows indicate the Stefan-Boltzmann limits.

that depends only on the link variables. The lattice representation of the partition function is

$$Z = \int \prod_{n,\mu} dU_\mu(n) \det(M(U)) e^{-S}, \tag{45}$$

where $M(U)$ is the fermion matrix. The partition function depends on the number of lattice sites N_τ, N_σ, the bare coupling constant g, and the dimensionless quark masses ma.

Note that the partition function has no explicit dependence on the lattice spacing. Asymptotic freedom implies that the bare coupling should go to zero as $a \to 0$ and the continuum limit corresponds to $g \to 0$. Asymptotically

$$a\Lambda_{lat} = \exp(-8\pi^2/(bg^2)), \tag{46}$$

where b is the first coefficient of the beta function, see equ. (4), and Λ_{lat} is the QCD scale parameter on the lattice. Λ_{lat} can be related to the continuum scale parameter by a perturbative calculation [37]. In practice the lattice spacing is not small to enough to use the perturbative result

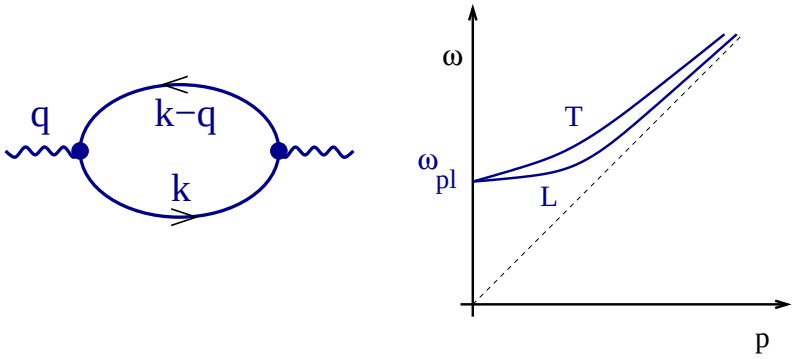

Figure 5. One loop contribution to the photon polarization tensor (left panel) and plasmon dispersion relation in a hot QED plasma.

equ. (46) and a is determined by from a physical quantity like the string tension or the rho meson mass. Once the lattice spacing is known the temperature is determined by $T = 1/(N_\tau a)$.

Lattice results for the order parameter and the equation of state are shown in Figs. (3,4). Current results for the transition temperature are [43]

$$T_c(N_f = 2) = (173 \pm 8) \text{ MeV}, \quad T_c(N_f = 0) = (271 \pm 2) \text{ MeV}, \tag{47}$$

where the errors are purely statistical. The equation of state shows a rapid rise in the pressure near T_c, but the pressure remains significantly below the free gas limit even at $T \sim (2-3)T_c$.

3.5. *Perturbative QCD*

At temperatures significantly above T_c quarks and gluons are weakly coupled and perturbative methods are expected to be useful. The starting point of the perturbative expansion at non-zero temperature is the path integral representation of the QCD partition function given in equ. (40). The only difference as compared to the zero temperature result is the fact that the fields satisfy periodic boundary conditions in imaginary time. Consider the Fourier representation of the gluon field

$$A_\mu(\vec{x}, \tau) = \sum_n \int d^3k \; A^n_\mu(\vec{k}) e^{-i(\vec{k}\vec{x} + \omega_n \tau)}. \tag{48}$$

We can also write down an analogous expansion for fermions. The boundary conditions imply that the allowed frequencies, called the Matsubara

frequencies, are discrete. We have

$$\begin{array}{ll} \omega_n = 2\pi n T & \text{bosons} \\ \omega_n = (2n+1)\pi T & \text{fermions} \end{array}. \tag{49}$$

The only change in the Feynman rules is that continuous energy variables are replaced by discrete Matsubara frequencies, $p_0 \to i\omega_n$, and that integrals over energy are replaced by discrete sums

$$\int \frac{d^4p}{(2\pi)^4} \to T\sum_n \int \frac{d^3p}{(2\pi)^3}. \tag{50}$$

Typical sums that appear in one-loop calculations in the Matsubara formalism are

$$\sum_k \frac{1}{x^2+k^2} = \frac{2\pi}{x}\left(\frac{1}{2} + \frac{1}{e^{2\pi x}-1}\right), \tag{51}$$

$$\sum_k \frac{1}{x^2+(2k+1)^2} = \frac{\pi}{x}\left(\frac{1}{2} - \frac{1}{e^{\pi x}+1}\right). \tag{52}$$

We observe that performing sums over Matsubara frequencies leads to Bose-Einstein and Fermi-Dirac distribution functions.

As an application of the finite temperature formalism we wish to study the one-loop correction to the gluon propagator in a hot QCD medium. For simplicity we begin with the analogous problem in a hot QED plasma. The photon polarization function is (see Fig. 5)

$$\Pi_{\mu\nu}(q) = e^2 T \sum_n \int \frac{d^3k}{(2\pi)^3} \mathrm{tr}[\gamma_\mu \not{k} \gamma_\nu (\not{k} - \not{q})]\Delta(k)\Delta(k-q), \tag{53}$$

where $\Delta(k) = \omega_n^2 + \vec{k}^2$. Using identities like equ. (52) we can decompose the integral into a $T = 0$ and a finite temperature part. In the following we will only consider the $T \neq 0$ terms. Thermal corrections to the photon propagator become important when the photon momentum is much smaller than the temperature. In this case we can assume that the loop momenta are on the order of T. This is called the hard thermal loop (HTL) approximation [44]. The photon polarization function in the HTL approximation is

$$\Pi_{\mu\nu} = 2m^2 \int \frac{d\Omega}{4\pi}\Big(\frac{i\omega \hat{K}_\mu \hat{K}_\nu}{q\cdot\hat{K}} + \delta_{\mu 0}\delta_{\nu 0}\Big), \tag{54}$$

where $m^2 = e^2T^2/6$, $\hat{K} = (-i, \hat{k})$ and $d\Omega$ is an integral over the direction of $\hat{k}$. In the case of the gluon propagator in QCD there are extra graphs

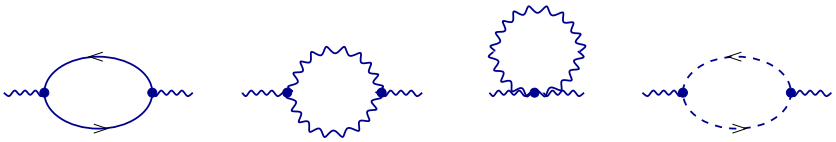

Figure 6. One loop contribution to the gluon polarization tensor in the quark gluon plasma. Solid lines are quark propagators, wavy lines are gluons, and dashed lines are ghosts.

generated by the three and four-gluon vertices as well as ghost contributions but, remarkably, the structure of the HTL polarization function is unchanged. In QCD the parameter m^2 is given by $m^2 = g^2T^2(1 + N_f/6)$.

Insertions of the polarization function into the photon (gluon) propagator form a simple geometric series. The resummed photon propagator is

$$D_{\mu\nu} = \frac{1}{(D^0_{\mu\nu})^{-1} + \Pi_{\mu\nu}}. \tag{55}$$

This result can be used to study the interaction between two charges in the plasma. The Coulomb interaction is determined by the Fourier transform of the static propagator

$$V(r) = e \int \frac{d^3q}{(2\pi)^3} \frac{e^{iqr}}{\vec{q}^2 + \Pi_{00}} \simeq -\frac{e}{r} \exp(-m_D r), \tag{56}$$

where $m_D^2 = 2m^2$ is the Debye mass and we have used $\Pi_{00}(0, \vec{q} \to 0) = m_D^2$. Equ. (56) shows that the Coulomb interaction is screened at distances $r \sim m_D^{-1} \sim (eT)^{-1}$. The mechanism for charge screening is easy to understand. A test charge polarizes the electron-positron plasma, and the polarization cloud screens the charge. Note that the typical distance between charges is $r \sim T^{-1} \ll r_D$ and Debye screening is a collective effect that involves many charge carriers.

The magnetic interaction is not screened, $\Pi_{ii}(0, \vec{q} \to 0) = 0$. However, if the photon energy is finite the polarization develops an imaginary part

$$\mathrm{Im}\Pi_{ii}(\omega, q) \sim \frac{\omega}{q} m_D^2 \Theta(q - \omega), \tag{57}$$

and non-static exchanges are damped. This phenomenon is called Landau damping. The mechanism of Landau damping is a transfer of energy from the electromagnetic field to electrons and positrons in the plasma. The absence of magnetic screening implies that the static magnetic sector of

the QCD plasma remains non-perturbative even if the temperature is very high.

In order to study the propagation of collective modes in the plasma in more detail it is useful to split the polarization tensor into transverse and longitudinal components

$$\Pi_{\mu\nu}(q) = \Pi^T(q) P^T_{\mu\nu} + \Pi^L(q) P^L_{\mu\nu} \tag{58}$$

$$P^T_{ij} = \delta_{ij} - \hat{q}_i \hat{q}_j, \qquad P^T_{00} = P^T_{0i} = 0, \tag{59}$$

$$P^L_{\mu\nu} = -g_{\mu\nu} + \frac{q_\mu q_\nu}{q^2} - P^T_{\mu\nu}. \tag{60}$$

We can study the propagation of photons by identifying the poles of the transverse and longitudinal components of the photon propagator, see Fig. 5. We observe that for large momenta $|\vec{q}| \gg m$ the dispersion relation is not strongly affected by the medium. In this limit we also find that the longitudinal mode has an exponentially small residue. As $\vec{q} \to 0$ the energy of both longitudinal and transverse modes approach the plasma frequency $\omega_{pl} = \sqrt{2/3}\, m$.

4. QCD at Small Density: Nuclear Matter

4.1. *Introduction*

In this section we study hadronic matter at non-zero baryon density. In QCD the numbers of all quark flavors are conserved individually. Once the weak interaction is taken into account only baryon number and electric charge are conserved. Bulk matter has to be electrically neutral because the Coulomb energy of a charged system diverges in the infinite volume limit. In hadronic matter neutrality can be achieved by balancing the charge density in hadrons, which is usually positive, by a finite density of electrons.

The partition function of QCD at non-zero baryon chemical potential is given by

$$Z = \sum_i \exp\left(-\frac{E_i - \mu N_i}{T}\right), \tag{61}$$

where i labels all quantum states of the system, E_i and N_i are the energy and baryon number of the state i. If the temperature and chemical potential are both zero then only the ground state contributes to the partition function. All other states give exponentially small contributions. QCD has a massgap for states with non-zero baryon number. This means that there

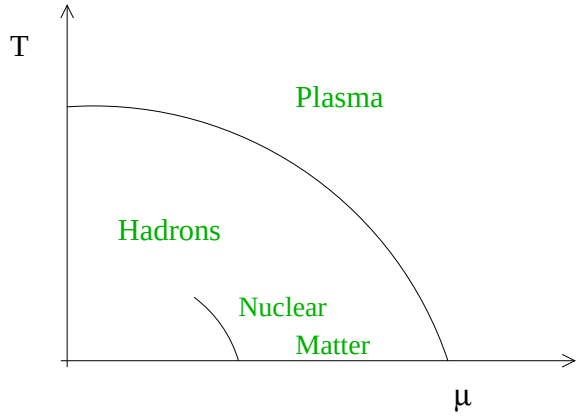

Figure 7. Naive phase diagram of hadronic matter as a function of the baryon chemical potential and temperature.

is an onset chemical potential

$$\mu_{onset} = \min_i(E_i/N_i), \tag{62}$$

such that the partition function is independent of μ for $\mu < \mu_{onset}$. For $\mu > \mu_{onset}$ the baryon density is non-zero. If the chemical potential is just above the onset chemical potential we can describe QCD, to first approximation, as a dilute gas of non-interacting nucleons. In this approximation $\mu_{onset} = m_N$. Of course, the interaction between nucleons is essential. Without it, we would not have stable nuclei. As a consequence, nuclear matter is self-bound and the energy per baryon in the ground state is given by

$$\frac{E_N}{N} - m_N \simeq -15\,\mathrm{MeV}. \tag{63}$$

The onset transition is a first order transition at which the baryon density jumps from zero to nuclear matter saturation density, $\rho_0 \simeq 0.14\,\mathrm{fm}^{-3}$. The first order transition continues into the finite temperature plane and ends at a critical endpoint at $T = T_c \simeq 10$ MeV, see Fig. 7.

Nuclear matter is a complicated many-body system and, unlike the situation at zero density and finite temperature, there is little information from numerical simulations on the lattice. This is related to the so-called 'sign problem'. At non-zero chemical potential the path integral representation of the partition function is

$$Z = \int dA_\mu \det(i\not{D} + i\mu\gamma_4)e^{-S} = \int dA_\mu e^{i\phi}|\det(i\not{D} + i\mu\gamma_4)|e^{-S}, \tag{64}$$

where ϕ is the complex phase of the fermion determinant. Since the determinant is complex standard Monte-Carlo techniques based on importance sampling fail. Recently, some progress has been made in simulating QCD for small μ and $T \simeq T_c$ [45,46,47], but the regime of small temperature remains inaccessible.

However, if the density is very much larger than nuclear matter saturation density, $\rho \gg \rho_0$, we expect the problem to simplify. In this regime it is natural to use a system of non-interacting quarks as a starting point [31]. The low energy degrees of freedom are quark excitations and holes in the vicinity of the Fermi surface. Since the Fermi momentum is large, asymptotic freedom implies that the interaction between quasi-particles is weak. As a consequence, the naive expectation is that chiral symmetry is restored and quarks and gluons are deconfined. It seems natural to assume that the quark liquid at high baryon density is continuously connected to the quark-gluon plasma at high temperature. These naive expectations are summarized in the phase diagram shown in Fig. 7.

4.2. *Fermi liquids*

Before we study the high density phase in more detail we would like to discuss systems of nucleons at low density. For simplicity we will begin with pure neutron matter at densities below nuclear matter saturation density. This problem is relevant to the behavior of matter near the surface of a neutron star, which is at subnuclear densities and has a large neutron-to-proton ratio. We will also see that pure neutron matter exhibits some very interesting universal features which can be studied experimentally using trapped atomic gases.

If the density is low then the typical momenta are small and neither the structure of the neutron nor the details of the neutron-neutron interaction are important. This means that the system can be described by an effective lagrangian of pointlike nucleons interacting via a short-range interaction [8,48]. The lagrangian is

$$\mathcal{L}_0 = \psi^\dagger \left(i\partial_0 + \frac{\nabla^2}{2m} \right) \psi - \frac{C_0}{2} \left(\psi^\dagger \psi \right)^2 . \tag{65}$$

The coupling constant C_0 is related to the scattering length, $C_0 = 4\pi a/m$. Note that $C_0 > 0$ corresponds to a repulsive interaction, and $C_0 < 0$ is an attractive interaction. The lagrangian equ. (65) is invariant under the $U(1)$ transformation $\psi \to e^{i\phi}\psi$. The $U(1)$ symmetry implies that the fermion

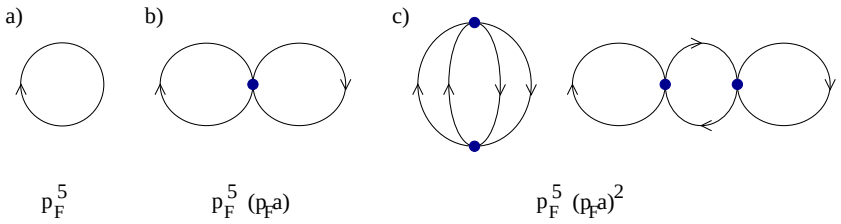

Figure 8. Leading order Feynman diagrams for the ground state energy of a dilute gas of fermions interacting via a short range potential.

number

$$N = \int d^3x\, \psi^\dagger \psi \tag{66}$$

is conserved. We introduce a chemical potential μ conjugate to the fermion number N and study the partition function

$$Z(\mu, \beta) = \mathrm{Tr}\left[e^{-\beta(H-\mu N)}\right]. \tag{67}$$

Here, H is the Hamiltonian associated with $\mathcal{L}$ and $\beta = 1/T$ is the inverse temperature. The average number of particles for a given chemical potential μ and temperature T is given by $\langle N\rangle = T(\partial \log Z)/(\partial\mu)$. At zero temperature the chemical potential is the energy required to add one particle to the system.

We observe that the chemical potential simply shifts the energy in the lagrangian. This implies that we have to carefully analyze the boundary conditions in the path integral in order to fix the pole prescription. The correct Minkowski space propagator is

$$S^0_{\alpha\beta}(p) = \frac{\delta_{\alpha\beta}}{p_0 - \epsilon_p + i\delta\mathrm{sgn}(\epsilon_p)} = \delta_{\alpha\beta}\left\{\frac{\Theta(p-p_F)}{p_0 - \epsilon_p + i\delta} + \frac{\Theta(p_F - p)}{p_0 - \epsilon_p - i\delta}\right\}, \tag{68}$$

where $\epsilon_p = E_p - \mu$, $E_p = \vec{p}^{\,2}/(2m)$ and $\delta \to 0^+$. The quantity $p_F = \sqrt{2m\mu}$ is called the Fermi momentum. The two terms in equ. (68) have a simple physical interpretation. At finite density and zero temperature all states with momenta below the Fermi momentum are occupied, while all states above the Fermi momentum are empty. The possible excitation of the system are particles above the Fermi surface or holes below the Fermi surface, corresponding to the first and second term in equ. (68). The particle density is given by

$$\frac{N}{V} = \int \frac{d^4p}{(2\pi)^4} S^0_{\alpha\alpha}(p)\, e^{ip_0\eta}\big|_{\eta\to 0^+} = 2\int \frac{d^3p}{(2\pi)^3}\Theta(p_F - p) = \frac{p_F^3}{3\pi^2}. \tag{69}$$

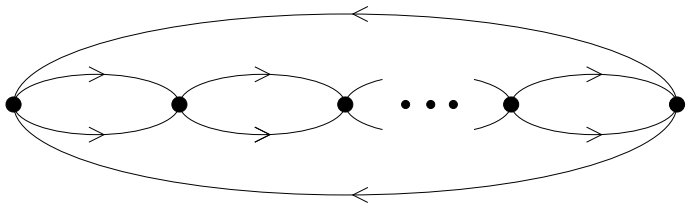

Figure 9. Particle-particle ladder diagrams for the ground state energy of a dilute gas of fermions.

As a first simple application we can compute the energy density as a function of the fermion density. For free fermions, we find

$$\mathcal{E} = 2 \int \frac{d^3p}{(2\pi)^3} E_p \Theta(p_F - p) = \frac{3}{5} \frac{p_F^2}{2m} \frac{N}{V}. \tag{70}$$

We can also compute the corrections to the ground state energy due to the interaction $\frac{1}{2}C_0(\psi^\dagger\psi)^2$. The first term is a two-loop diagram with one insertion of C_0, see Fig. 8. We have

$$\mathcal{E}_1 = C_0 \left(\frac{p_F^3}{6\pi^2} \right)^2. \tag{71}$$

We should note that equ. (71) contains two possible contractions, called the direct and the exchange term. If the fermions have spin s and degeneracy $g = (2s+1)$ then equ. (71) has to be multiplied by a factor $g(g-1)/2$. We also note that the sum of the first two terms in the energy density can be written as

$$\frac{E}{N} = \frac{p_F^2}{2m} \left(\frac{3}{5} + \frac{2}{3\pi}(p_F a) + \dots \right), \tag{72}$$

which shows that the C_0 term is the first term in an expansion in $p_F a$, suitable for a dilute, weakly interacting, Fermi gas. The expansion in $(p_F a)$ was carried out to order $(p_F a)^2$ by Huang, Lee and Yang [49,50]. Since then, the accuracy was pushed to [7,48] $O((p_F a)^4 \log(p_F a))$.

4.3. *Unitary Limit*

The neutron-neutron scattering length is very large, $a_{nn} = -18$ fm, and the $(p_F a)$ expansion is not particularly useful. Indeed, since the scattering length is so much larger than all other hadronic length scales it makes sense to consider the opposite limit and take the scattering length to infinity. This means that there is a bound state right at threshold and that the low energy

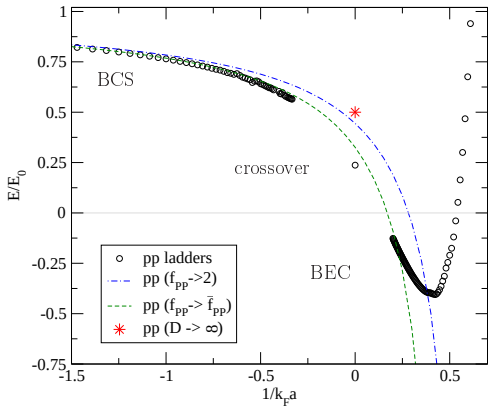

Figure 10. Total energy of an interacting fermion gas in units of the energy of a free fermion gas as a function of $(k_F a)^{-1}$. The open circles show the result of a numerical calculation of particle-particle ladder diagrams. The dashed curve shows the approximations given in equ. (74). The star is the result of the $d \to \infty$ calculation in the unitary limit.

cross section saturates the unitarity bound. If neutron matter is dilute then we can also assume that $(p_F r) \ll 1$, where r is the range of the potential. In this limit the only energy scale in the problem is $p_F^2/(2m)$ and the energy per particle is

$$\frac{E}{N} = \xi \frac{3}{5} \frac{p_F^2}{2m}, \tag{73}$$

where ξ is an unknown parameter. Comparison with equ. (70) shows that for free fermions $\xi = 1$.

Neutron matter in the unitary limit is very strongly correlated and the determination of ξ is a complicated, non-perturbative problem. However, since ξ is insensitive to the details of the interaction the result is the same for any dilute Fermi gas with a two-body bound state near threshold. It is now possible to create such a system in the laboratory by trapping cold fermionic atoms. In these systems the scattering length can be controlled using Feshbach resonances induced by an external magnetic field. A recent experimental analysis yields the value [51] $\xi \simeq 0.45$.

There have been a number of theoretical attempts to determine ξ. Since the two-body interaction is large it is natural to begin with the sum of all

two-body diagrams, see Fig. 9. This sum gives [52]

$$\frac{E}{N} = \frac{p_F^2}{2M}\left\{\frac{3}{5} + \frac{2(k_F a)/(3\pi)}{1 - \frac{6}{35\pi}(11 - 2\log(2))(p_F a)}\right\}. \tag{74}$$

from which we deduce $\xi \simeq 0.32$. This is reasonably close to the experimental result, but since the system is strongly correlated there is no obvious reason to restrict ourselves to two-body ladders. We have recently studied the possibility that equ. (74) can be justified as the leading term in an expansion in $1/d$, where d is the number of space dimensions [53,52]. This approach appears promising, but $1/d$ corrections have not been worked out yet. Another possibility is to pursue numerical approaches. Green function Monte Carlo calculations give $\xi = 0.44$, in very good agreement with the experimental result [54]. Several groups have performed euclidean lattice calculations[55,56,57,58], similar to the lattice QCD calculations discussed in Sect. 3.4. These calculations do not suffer from a sign problem and can be extended to finite temperature.

4.4. *Nuclear Matter and Chiral Restoration*

Ordinary nuclei consist of roughly equal numbers of neutrons and protons. In order to study heavy nuclei it is useful to consider nuclear matter in pure QCD, i.e. ignoring the contribution from electrons as well as the Coulomb repulsion between protons. As discussed in Sect. 4.1 nuclear matter saturates at a density $\rho_0 \simeq 0.15\,\mathrm{fm}^{-3}$. The binding energy of nuclear matter is $B/A \simeq 15$ MeV. Numerical calculations based on realistic nucleon-nucleon potentials are successful in reproducing these numbers, but we do not understand very well why nuclear matter saturates and how the saturation density and the binding energy are related to more fundamental properties of QCD.

We also do not know very well how to extrapolate the equation of state beyond the saturation density. An important question is whether we expect chiral symmetry to be restored as the density increases. If the density is small this question can be studied using the method we employed in Sect. 3.1. The quark condensate is given by

$$\langle \bar{q}q \rangle_\rho = T\frac{\partial}{\partial m_q}\log Z. \tag{75}$$

The partition function of a dilute gas of protons and neutrons is

$$\log Z = 4\int \frac{d^3p}{(2\pi)^3}\log\left(1 + e^{-(E_N-\mu)/T}\right). \tag{76}$$

The quark mass dependence of the nucleon mass is related to πN Sigma term $\Sigma_{\pi N} = m_q \partial m_N / \partial m_q$. We get

$$\langle \bar{q}q \rangle_\rho = 4 \int \frac{d^3p}{(2\pi)^3} \frac{M_N}{E_N} \Big(\frac{\partial M_N}{\partial m_q} \Big) \Theta(p_F - |\vec{p}|) = \langle \bar{q}q \rangle_0 \Big\{ 1 - \frac{\Sigma_{\pi N} \rho_0}{m_\pi^2 f_\pi^2} \Big(\frac{\rho}{\rho_0} \Big) \Big\}. \tag{77}$$

The Sigma term can be extracted in pion-nucleon scattering. Using $\Sigma_{\pi N} \simeq 45$ MeV we find

$$\langle \bar{q}q \rangle_\rho \simeq \langle \bar{q}q \rangle_0 \Big\{ 1 - \frac{1}{3} \Big(\frac{\rho}{\rho_0} \Big) \Big\}, \tag{78}$$

which indicates that chiral condensate is significantly modified already at nuclear matter saturation density.

4.5. *Superfluidity*

One of the most remarkable phenomena that take place in many body systems is superfluidity. Superfluidity is related to an instability of the Fermi surface in the presence of attractive interactions between fermions. Let us consider fermion-fermion scattering in the simple model introduced in Sect. 4.2. At leading order the scattering amplitude is given by

$$\Gamma_{\alpha\beta\gamma\delta}(p_1, p_2, p_3, p_4) = C_0 \left(\delta_{\alpha\gamma}\delta_{\beta\delta} - \delta_{\alpha\delta}\delta_{\beta\gamma} \right). \tag{79}$$

At next-to-leading order we find the corrections shown in Fig. 11. A detailed discussion of the role of these corrections can be found in [8,59,60]. The BCS diagram is special, because in the case of a spherical Fermi surface it can lead to an instability in weak coupling. The main point is that if the incoming momenta satisfy $\vec{p}_1 \simeq -\vec{p}_2$ then there are no kinematic restrictions on the loop momenta. As a consequence, all back-to-back pairs can mix and there is an instability even in weak coupling.

For $\vec{p}_1 = -\vec{p}_2$ and $E_1 = E_2 = E$ the BCS diagram is given by

$$\Gamma_{\alpha\beta\gamma\delta} = C_0^2 \left(\delta_{\alpha\gamma}\delta_{\beta\delta} - \delta_{\alpha\delta}\delta_{\beta\gamma} \right) \int \frac{d^4q}{(2\pi)^4} \frac{1}{E + q_0 - \epsilon_q + i\delta \mathrm{sgn}(\epsilon_q)} \frac{1}{E - q_0 - \epsilon_q + i\delta \mathrm{sgn}(\epsilon_q)}. \tag{80}$$

The loop integral has an infrared divergence near the Fermi surface as $E \to 0$. The scattering amplitude is proportional to

$$\Gamma_{\alpha\beta\gamma\delta} = \left(\delta_{\alpha\gamma}\delta_{\beta\delta} - \delta_{\alpha\delta}\delta_{\beta\gamma} \right) \left\{ C_0 - C_0^2 \left(\frac{p_F m}{2\pi^2} \right) \log \left(\frac{E_0}{E} \right) \right\}, \tag{81}$$

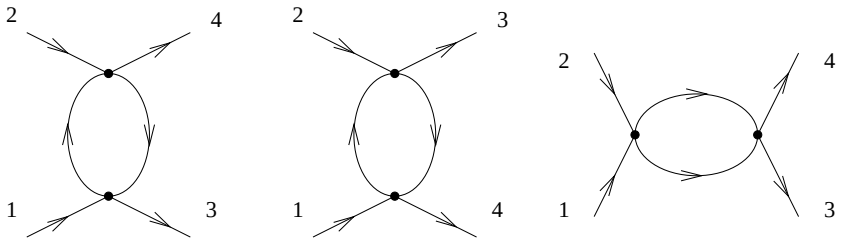

Figure 11. Second order diagrams that contribute to particle-particle scattering. The three diagrams are known as ZS (zero sound), ZS' and BCS (Bardeen-Cooper-Schrieffer) contribution.

where E_0 is an ultraviolet cutoff. Equ. (81) can be interpreted as an effective energy dependent coupling that satisfies the renormalization group equation [59,60]

$$E\frac{dC_0}{dE} = C_0^2\left(\frac{p_F m}{2\pi^2}\right), \tag{82}$$

with the solution

$$C_0(E) = \frac{C_0(E_0)}{1 + NC_0(E_0)\log(E_0/E)}, \tag{83}$$

where $N = (p_F m)/(2\pi^2)$ is the density of states. Equ. (83) shows that there are two possible scenarios. If the initial coupling is repulsive, $C_0(E_0) > 0$, then the renormalization group evolution will drive the effective coupling to zero and the Fermi liquid is stable. If, on the other hand, the initial coupling is attractive, $C_0(E_0) < 0$, then the effective coupling grows and reaches a Landau pole at

$$E_{crit} \sim E_0 \exp\left(-\frac{1}{N|C_0(E_0)|}\right). \tag{84}$$

At the Landau pole the Fermi liquid description has to break down. The renormalization group equation does not determine what happens at this point, but it seems natural to assume that the strong attractive interaction will lead to the formation of a fermion pair condensate. The fermion condensate $\langle \epsilon^{\alpha\beta}\psi_\alpha\psi_\beta\rangle$ signals the breakdown of the $U(1)$ symmetry and leads to a gap Δ in the single particle spectrum.

The scale of the gap is determined by the position of the Landau pole, $\Delta \sim E_{crit}$. A more quantitative estimate of the gap can be obtained in the mean field approximation. In the path integral formulation the mean field

approximation is most easily introduced using the Hubbard-Stratonovich trick. For this purpose we first rewrite the four-fermion interaction as

$$\frac{C_0}{2}(\psi^\dagger\psi)^2 = \frac{C_0}{4}\left\{(\psi^\dagger\sigma_2\psi^\dagger)(\psi\sigma_2\psi) + (\psi^\dagger\sigma_2\vec{\sigma}\psi^\dagger)(\psi\vec{\sigma}\sigma_2\psi)\right\}, \tag{85}$$

where we have used the Fierz identity $2\delta^{\alpha\beta}\delta^{\gamma\rho} = \delta^{\alpha\rho}\delta^{\gamma\beta} + (\vec{\sigma})^{\alpha\rho}(\vec{\sigma})^{\gamma\beta}$. Note that the second term in equ. (85) vanishes because $(\sigma_2\vec{\sigma})$ is a symmetric matrix. We now introduce a factor of unity into the path integral

$$1 = \frac{1}{Z_\Delta}\int D\Delta \exp\left(\frac{\Delta^*\Delta}{C_0}\right), \tag{86}$$

where we assume that $C_0 < 0$. We can eliminate the four-fermion term in the lagrangian by a shift in the integration variable Δ. The action is now quadratic in the fermion fields, but it involves a Majorana mass term $\psi\sigma_2\Delta\psi + h.c.$ The Majorana mass terms can be handled using the Nambu-Gorkov method. We introduce the bispinor $\Psi = (\psi, \psi^\dagger\sigma_2)$ and write the fermionic action as

$$S = \frac{1}{2}\int \frac{d^4p}{(2\pi)^4}\Psi^\dagger \begin{pmatrix} p_0 - \epsilon_p & \Delta \\ \Delta^* & p_0 + \epsilon_p \end{pmatrix}\Psi. \tag{87}$$

Since the fermion action is quadratic we can integrate the fermion out and obtain the effective lagrangian

$$L = \frac{1}{2}\mathrm{Tr}\left[\log\left(G_0^{-1}G\right)\right] + \frac{1}{C_0}|\Delta|^2, \tag{88}$$

where G is the fermion propagator

$$G(p) = \frac{1}{p_0^2 - \epsilon_p^2 - |\Delta|^2}\begin{pmatrix} p_0 + \epsilon_p & \Delta^* \\ \Delta & p_0 - \epsilon_p \end{pmatrix}. \tag{89}$$

The diagonal and off-diagonal components of $G(p)$ are sometimes referred to as normal and anomalous propagators. Note that we have not yet made any approximation. We have converted the fermionic path integral to a bosonic one, albeit with a very non-local action. The mean field approximation corresponds to evaluating the bosonic path integral using the saddle point method. Physically, this approximation means that the order parameter does not fluctuate. Formally, the mean field approximation can be justified in the large N limit, where N is the number of fermion fields. The saddle point equation for Δ gives the gap equation

$$\Delta = |C_0|\int \frac{d^4p}{(2\pi)^4}\frac{\Delta}{p_0^2 - \epsilon_p^2 - \Delta^2}. \tag{90}$$

Performing the p_0 integration we find

$$1 = \frac{|C_0|}{2} \int \frac{d^3p}{(2\pi)^3} \frac{1}{\sqrt{\epsilon_p^2 + \Delta^2}}. \tag{91}$$

Since $\epsilon_p = E_p - \mu$ the integral in equ. (91) has an infrared divergence on the Fermi surface $|\vec{p}| \sim p_F$. As a result, the gap equation has a non-trivial solution even if the coupling is arbitrarily small. The magnitude of the gap is $\Delta \sim \Lambda \exp(-1/(|C_0|N))$ where Λ is a cutoff that regularizes the integral in equ. (91) in the ultraviolet. If we treat equ. (65) as a low energy effective field theory we should be able to eliminate the unphysical dependence of the gap on the ultraviolet cutoff, and express the gap in terms of a physical observable. At low density this can be achieved by observing that the gap equation has the same UV behavior as the Lipmann-Schwinger equation that determines the scattering length at zero density

$$\frac{mC_0}{4\pi a} - 1 = \frac{C_0}{2} \int \frac{d^3p}{(2\pi)^3} \frac{1}{E_P}. \tag{92}$$

Combining equs. (91) and (92) we can derive an UV finite gap equation that depends only on the scattering length,

$$-\frac{m}{4\pi a} = \frac{1}{2} \int \frac{d^3p}{(2\pi)^3} \Big\{ \frac{1}{\sqrt{\epsilon_p^2 + \Delta^2}} - \frac{1}{E_p} \Big\}. \tag{93}$$

Solving for the Δ we find [61,62]

$$\Delta = \frac{8E_f}{e^2} \exp\left(-\frac{\pi}{2p_F|a|} \right). \tag{94}$$

Higher order corrections reduce the pre-exponent in this result by a factor $(4e)^{1/3} \simeq 2.2$ [63]. Like the perturbative calculation of the energy per particle this result is not very useful for neutron matter, since the scattering length is very large. Taking higher order corrections into account, Equ. (94) suggests that $\Delta \sim 0.49E_f$ as $p_F|a| \to \infty$. Surprisingly, this estimate agrees very well with numerical calculations [64]. The gap is also quite sensitive to the effective range of the interaction. Calculations based on potential models give gaps on the order of 2 MeV at nuclear matter density.

4.6. *Landau-Ginzburg theory*

In neutron stars there is not only pairing between neutrons but also pairing between protons. Since protons carry charge this implies that the material

is not only a superfluid but also a superconductor. Superconductors have many interesting properties which can be understood from the symmetries involved. We will consider a system of protons coupled to a $U(1)$ gauge field A_μ. The order parameter $\Phi = \langle \epsilon^{\alpha\beta}\psi_\alpha\psi_\beta\rangle$ breaks $U(1)$ invariance. Consider a gauge transformation

$$A_\mu \to A_\mu + \partial_\mu \Lambda. \tag{95}$$

The order parameter transforms as

$$\Phi \to \exp(2ie\Lambda)\Phi. \tag{96}$$

The breaking of gauge invariance is responsible for most of the unusual properties of superconductors [65,66]. This can be seen by constructing the low energy effective action of a superconductor. For this purpose we write the order parameter in terms of its modulus and phase

$$\Phi(x) = \exp(2ie\phi(x))\tilde{\Phi}(x). \tag{97}$$

The field ϕ corresponds to the Goldstone mode. Under a gauge transformation $\phi(x) \to \phi(x) + \Lambda(x)$. Gauge invariance restricts the form of the effective Lagrange function

$$L = -\frac{1}{4}\int d^3x\, F_{\mu\nu}F_{\mu\nu} + L_s(A_\mu - \partial_\mu\phi). \tag{98}$$

There is a large amount of information we can extract even without knowing the explicit form of L_s. Stability implies that $A_\mu = \partial_\mu\phi$ corresponds to a minimum of the energy. This means that up to boundary effects the gauge potential is a total divergence and that the magnetic field has to vanish. This phenomenon is known as the Meissner effect.

Equ. (98) also implies that a superconductor has zero resistance. The equations of motion relate the time dependence of the Goldstone boson field to the potential,

$$\dot{\phi}(x) = -V(x). \tag{99}$$

The electric current is related to the gradient of the Goldstone boson field. Equ. (99) shows that the time dependence of the current is proportional to the gradient of the potential. In order to have a static current the gradient of the potential has to be constant throughout the sample, and the resistance is zero.

In order to study the properties of a superconductor in more detail we have to specify L_s. For this purpose we assume that the system is

time-independent, that the spatial gradients are small, and that the order parameter is small. In this case we can write

$$L_s = \int d^3x \left\{ -\frac{1}{2} \left| \left(\nabla - 2ie\vec{A} \right) \Phi \right|^2 + \frac{1}{2} m_H^2 \left(\Phi^* \Phi \right)^2 - \frac{1}{4} g \left(\Phi^* \Phi \right)^4 + \ldots \right\}, \tag{100}$$

where m_H and g are unknown parameters that depend on the temperature. Equ. (100) is known as the Landau-Ginzburg effective action. Strictly speaking, the assumption that the order parameter is small can only be justified in the vicinity of a second order phase transition. Nevertheless, the Landau-Ginzburg description is instructive even in the regime where $t = (T - T_c)/T_c$ is not small. It is useful to decompose $\Phi = \rho \exp(2ie\phi)$. For constant fields the effective potential,

$$V(\rho) = -\frac{1}{2} m_H^2 \rho^2 + \frac{1}{4} g \rho^4, \tag{101}$$

is independent of ϕ. The minimum is at $\rho_0^2 = m_H^2/g$ and the energy density at the minimum is given by $E = -m_H^4/(4g)$. This shows that the two parameters m_H and g can be related to the expectation value of Φ and the condensation energy. We also observe that the phase transition is characterized by $m_H(T_c) = 0$.

In terms of ϕ and ρ the Landau-Ginzburg action is given by

$$L_s = \int d^3x \left\{ -2e^2 \rho^2 \left(\vec{\nabla}\phi - \vec{A} \right)^2 + \frac{1}{2} m_H^2 \rho^2 - \frac{1}{4} g \rho^4 - \frac{1}{2} \left(\nabla \rho \right)^2 \right\}. \tag{102}$$

The equations of motion for $\vec{A}$ and ρ are given by

$$\vec{\nabla} \times \vec{B} = 4e^2 \rho^2 \left(\nabla\phi - \vec{A} \right), \tag{103}$$

$$\nabla^2 \rho = -m_H^2 \rho^2 + g\rho^3 + 4e^2 \rho \left(\vec{\nabla}\phi - \vec{A} \right). \tag{104}$$

Equ. (103) implies that $\nabla^2 \vec{B} = -4e^2 \rho^2 \vec{B}$. This means that an external magnetic field $\vec{B}$ decays over a characteristic distance $\lambda = 1/(2e\rho)$. Equ. (104) gives $\nabla^2 \rho = -m_H^2 \rho + \ldots$. As a consequence, variations in the order parameter relax over a length scale given by $\xi = 1/m_H$. The two parameters λ and ξ are known as the penetration depth and the coherence length.

The relative size of λ and ξ has important consequences for the properties of superconductors. In a type II superconductor $\xi < \lambda$. In this case magnetic flux can penetrate the system in the form of vortex lines. At the core of a vortex the order parameter vanishes, $\rho = 0$. In a type II material

the core is much smaller than the region over which the magnetic field goes to zero. The magnetic flux is given by

$$\int_A \vec{B}\cdot\vec{S} = \oint_{\partial A} \vec{A}\cdot d\vec{l} = \oint_{\partial A} \vec{\nabla}\phi\cdot d\vec{l} = \frac{n\pi\hbar}{e}, \tag{105}$$

and quantized in units of $\pi\hbar/e$. In a type II superconductor magnetic vortices repel each other and form a regular lattice known as the Abrikosov lattice. In a type I material, on the other hand, vortices are not stable and magnetic fields can only penetrate the sample if superconductivity is destroyed.

5. QCD at high density

5.1. *Color superconductivity*

In Sect. 4.1 we introduced a few simple arguments concerning the phase diagram of QCD in the $\mu - T$ plane. These arguments are summarized in Fig. 7. The basic idea is that large baryon density is just like high temperature: there is a large scale in the problem, the effective coupling is weak, and the system is described, to a good approximation, as a weakly interacting quark liquid. We expect, in particular, that quarks are deconfined and that chiral symmetry is restored.

We also showed, however, that systems at finite density, as exemplified by nuclear matter, have a very rich phase diagram. We saw, in particular, that the BCS instability will lead to pair condensation whenever there is an attractive fermion-fermion interaction, even if the interaction is weak. At very large density, the attraction is provided by one-gluon exchange between quarks in a color anti-symmetric $\bar{3}$ state. High density quark matter is therefore expected to behave as a color superconductor [67,68,69,70].

Color superconductivity is described by a pair condensate of the form

$$\Phi = \langle \psi^T C\Gamma_D \lambda_C \tau_F \psi\rangle. \tag{106}$$

Here, C is the charge conjugation matrix, and $\Gamma_D, \lambda_C, \tau_F$ are Dirac, color, and flavor matrices. Except in the case of only two colors, the order parameter cannot be a color singlet. Color superconductivity is therefore characterized by the breakdown of color gauge invariance. This statement has to be interpreted in the sense of Sect. 4.6. Gluons acquire a mass due to the (Meissner-Anderson) Higgs mechanism.

A rough estimate of the critical density for the transition from chiral symmetry breaking to color superconductivity, the superconducting gap

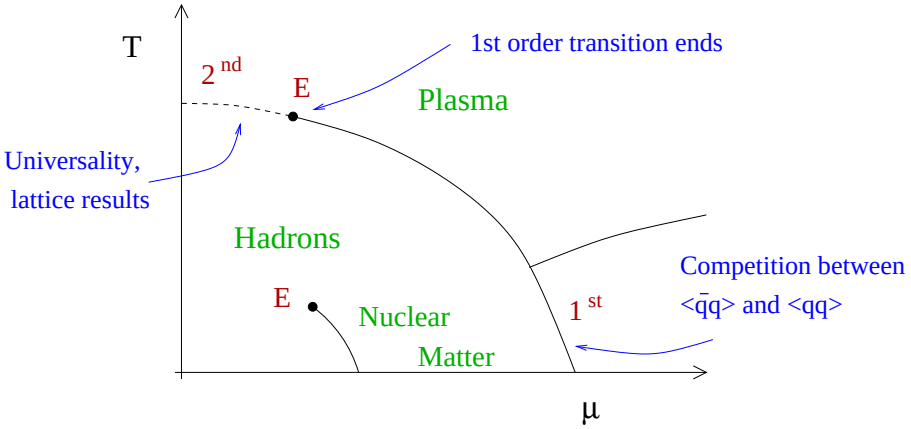

Figure 12. First revision of the phase diagram of hadronic matter. This figure shows the phase diagram of strongly interacting matter obtained from a mean field treatment of chiral symmetry breaking and color superconductivity in QCD with two flavors.

and the transition temperature is provided by schematic four-fermion models [71,72]. Typical models are based on the instanton interaction

$$\mathcal{L} = G_I \left\{ (\bar{\psi}\tau_\alpha^- \psi)^2 + (\bar{\psi}\gamma_5 \tau_\alpha^- \psi)^2 \right\}, \tag{107}$$

or a schematic one-gluon exchange interaction

$$\mathcal{L} = G_{OGE} \left(\bar{\psi}\gamma_\mu \frac{\lambda^a}{2} \psi \right)^2 . \tag{108}$$

Here $\tau_\alpha^- = (\vec{\tau}, i)$ is an isospin matrix and λ^a are the color Gell-Mann matrices. The strength of the four-fermion interaction is typically tuned to reproduce the magnitude of the chiral condensate and the pion decay constant at zero temperature and density. In the mean field approximation the effective quark mass associated with chiral symmetry breaking is determined by a gap equation of the type

$$M_Q = G_M \int^\Lambda \frac{d^3p}{(2\pi)^3} \frac{M_Q}{\sqrt{\vec{p}^2 + M_Q^2}} \left(1 - n_F(E_p)\right), \tag{109}$$

where G_M is the effective coupling in the quark-anti-quark channel, Λ is a cutoff, and $n_F(E)$ is the Fermi distribution. Both the instanton interaction and the one-gluon exchange interaction are attractive in the color anti-triplet scalar diquark channel $\epsilon^{abc}(\psi^b C\gamma_5 \psi^c)$. A pure one-gluon exchange interaction leads to a degeneracy between scalar and pseudoscalar

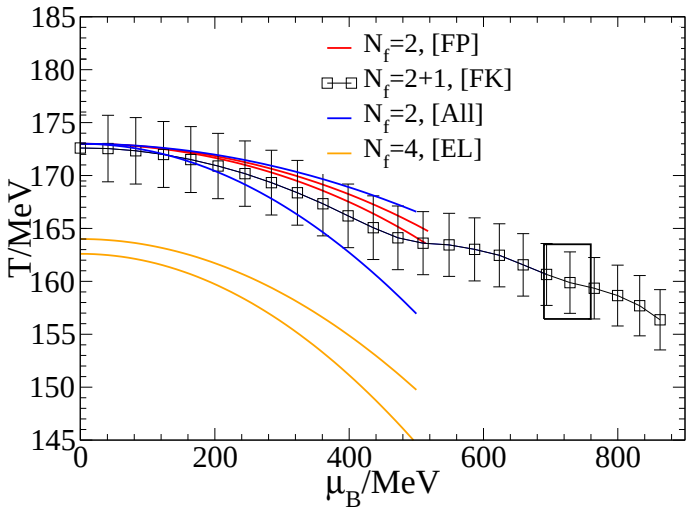

Figure 13. Location of the (pseudo) critical line and tri-critical point (box) as measured in different simulations, de Forcrand and Philipsen (2002) [FP], Fodor and Katz (2002) [FK], Allton et al (2002) [All], D'Ellia and Lombardo (2002) [EL]. Figure from de Forcrand and Philipsen (2003).

diquark condensation, but instantons are repulsive in the pseudoscalar diquark channel. The gap equation in the scalar diquark channel is

$$\Delta = \frac{G_D}{2} \int^{\Lambda} \frac{d^3p}{(2\pi)^3} \frac{\Delta}{\sqrt{(|\vec{p}| - p_F)^2 + \Delta^2}}, \tag{110}$$

where we have neglected terms that do not have a singularity on the Fermi surface $|\vec{p}| = p_F$. In the case of a four-fermion interaction with the quantum numbers of one-gluon exchange $G_D = G_M/(N_c - 1)$. The same result holds for instanton effects. In order to determine the correct ground state we have to compare the condensation energy in the chiral symmetry broken and diquark condensed phases. We have $E \sim f_\pi^2 M_Q^2$ in the $(\bar{q}q)$ condensed phase and $E \sim p_F^2 \Delta^2/(2\pi^2)$ in the (qq) condensed phase.

At zero temperature and density both equs. (109) and (110) only have non-trivial solutions if the coupling exceeds a critical value. Since $G_M > G_D$ we have $M_Q > \Delta$ and the energetically preferred solution corresponds to chiral symmetry breaking. If the density increases Pauli-Blocking in equ. (109) becomes important and the effective quark mass decreases. The diquark gap equation behaves very differently. Equ. (110) has an infrared singularity on the Fermi surface, $p = p_F$, and this singularity is multiplied

by a finite density of states, $N = p_F^2/(2\pi)^2$. As a consequence, there is a non-trivial solution even if the coupling is weak. The gap grows with density until the Fermi momentum becomes on the order of the cutoff. For realistic values of the parameters we find a first order transition for remarkably small values of the quark chemical potential, $\mu_Q \simeq 300$ MeV. The gap in the diquark condensed phase is $\Delta \sim 100$ MeV and the critical temperature is $T_c \sim 50$ MeV.

In the same model the finite temperature phase transition at zero baryon density is found to be of second order. This result is in agreement with universality arguments [73] and lattice results. If the transition at finite density and zero temperature is indeed of first order then the first order transition at zero baryon density has to end in a tri-critical point [74,75,76]. The tri-critical point is quite remarkable, because it remains a true critical point even if the quark masses are not zero. A non-zero quark mass turns the second order $T \neq 0$ transition into a smooth crossover, but the first order $\mu \neq 0$ transition persists. It is hard to predict where exactly the tri-critical point is located in the phase diagram. Recent lattice calculations suggest that the tri-critical point is sufficiently close to the finite temperature axis so that its location can be determined on the lattice, see Fig. 13. It may also be possible to locate the critical point experimentally. Heavy ion collisions at relativistic energies produce matter under the right conditions and experimental signatures of the tri-critical point have been suggested in [77].

A schematic phase diagram is shown in Fig. 12. We should emphasize that this phase diagram is based on simplified models and that there is no proof that the transition from nuclear matter to quark matter along the $T = 0$ line occurs via a single first order transition. Chiral symmetry breaking and color superconductivity represent two competing forms of order, and it seems unlikely that the two phases are separated by a second order transition. However, since color superconductivity modifies the spectrum near the Fermi surface, whereas chiral symmetry breaking operates near the surface of the Dirac sea, it is not clear that the two phases cannot coexist. Indeed, there are models in which a phase coexistence region appears [78].

5.2. *Phase structure in weak coupling*

5.2.1. *QCD with two flavors*

In this section we shall discuss how to use weak coupling methods in order to explore the phases of dense quark matter. We begin with what is usually

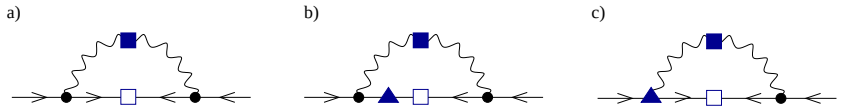

Figure 14. Fig. a) shows the leading contribution to the Dyson-Schwinger (gap) equation in QCD at finite density. The open square denotes an anomalous self energy (gap) insertion and the solid square is a gluon self energy insertion. Figs. b) and c) show quark self energy insertions and vertex corrections.

considered to be the simplest case, quark matter with two degenerate flavors, up and down. Renormalization group arguments suggest [79,80], and explicit calculations confirm [81,82], that whenever possible quark pairs condense in an s-wave state. This means that the spin wave function of the pair is anti-symmetric. Since the color wave function is also anti-symmetric, the Pauli principle requires the flavor wave function to be anti-symmetric too. This essentially determines the structure of the order parameter [71,72]

$$\Phi^a = \langle \epsilon^{abc} \psi^b C \gamma_5 \tau_2 \psi^c \rangle. \tag{111}$$

This order parameter breaks the color $SU(3) \to SU(2)$ and leads to a gap for up and down quarks with two out of the three colors. Chiral and isospin symmetry remain unbroken.

We can calculate the magnitude of the gap and the condensation energy using weak coupling methods. In weak coupling the gap is determined by ladder diagrams with the one gluon exchange interaction. These diagrams can be summed using the gap equation [83,84,85,86,87]

$$\Delta(p_4) = \frac{g^2}{12\pi^2} \int dq_4 \int d\cos\theta \left(\frac{\frac{3}{2} - \frac{1}{2}\cos\theta}{1 - \cos\theta + G/(2\mu^2)} + \frac{\frac{1}{2} + \frac{1}{2}\cos\theta}{1 - \cos\theta + F/(2\mu^2)} \right) \frac{\Delta(q_4)}{\sqrt{q_4^2 + \Delta(q_4)^2}}. \tag{112}$$

Here, $\Delta(p_4)$ is the frequency dependent gap, g is the QCD coupling constant and G and F are the self energies of magnetic and electric gluons. This gap equation is very similar to the BCS gap equation equ. (110) obtained in four-fermion models. The terms in the curly brackets arise from the magnetic and electric components of the gluon propagator. The numerators are the on-shell matrix elements $M_{ii,00} = [\bar{u}_h(p_1)\gamma_{i,0}u_h(p_3)][\bar{u}_h(p_2)\gamma_{i,0}u_h(p_4)]$ for the scattering of back-to-back fermions on the Fermi surface. The scattering angle is $\cos\theta = \hat{p}_1 \cdot \hat{p}_3$. In the case of a spin zero order parameter, the helicity h of all fermions is the same, see [84] for more detail.

The main difference between equ. (112) and the BCS gap equation (110) is that because the gluon is massless, the gap equation contains a collinear divergence for $\cos\theta \sim 1$. In a dense medium the collinear divergence is regularized by the gluon self energy. For $\vec{q} \to 0$ and to leading order in perturbation theory we have

$$F = 2m^2, \qquad G = \frac{\pi}{2} m^2 \frac{q_4}{|\vec{q}|}, \tag{113}$$

with $m^2 = N_f g^2 \mu^2/(4\pi^2)$. In the electric part, $m_D^2 = 2m^2$ is the familiar Debye screening mass. In the magnetic part, there is no screening of static modes, but non-static modes are modes are dynamically screened due to Landau damping. This is completely analogous to the situation at finite temperature [88], see Sect. 3.5.

For small energies dynamic screening of magnetic modes is much weaker than Debye screening of electric modes. As a consequence, perturbative color superconductivity is dominated by magnetic gluon exchanges. Using equ. (113) we can perform the angular integral in equ. (112) and find

$$\Delta(p_4) = \frac{g^2}{18\pi^2} \int dq_4 \log\left(\frac{b\mu}{\sqrt{|p_4^2 - q_4^2|}}\right) \frac{\Delta(q_4)}{\sqrt{q_4^2 + \Delta(q_4)^2}}, \tag{114}$$

with $b = 256\pi^4 (2/N_f)^{5/2} g^{-5}$. We can now see why it was important to keep the frequency dependence of the gap. Because the collinear divergence is regulated by dynamic screening, the gap equation depends on p_4 even if the frequency is small. We can also see that the gap scales as $\exp(-c/g)$. The collinear divergence leads to a gap equation with a double-log behavior. Qualitatively

$$\Delta \sim \frac{g^2}{18\pi^2} \Delta \left[\log\left(\frac{\mu}{\Delta}\right)\right]^2, \tag{115}$$

from which we conclude that $\Delta \sim \exp(-c/g)$. Equ. (115) is not sufficiently accurate to determine the correct value of the constant c. A more detailed analysis shows that the gap on the Fermi surface is given by

$$\Delta_0 \simeq 512\pi^4 (2/N_f)^{5/2} b' \mu g^{-5} \exp\left(-\frac{3\pi^2}{\sqrt{2}g}\right). \tag{116}$$

The factor b' is related to non-Fermi liquid effects, see [89,90,91]. In perturbation theory $b' = \exp(-(\pi^2+4)(N_c-1)/16)$ [87,92,93]. The condensation energy is given by

$$\epsilon = -N_d \Delta_0^2 \left(\frac{\mu^2}{4\pi^2}\right), \tag{117}$$

where $N_d = 4$ is the number of condensed species. In the mean field approximation the critical temperature is $T_c/\Delta_0 = e^\gamma/\pi \simeq 0.56$, as in standard BCS theory [85]. Fluctuations of the gauge field drive the transition first order [70,94]. Surprisingly, gauge field fluctuations increase the critical temperature as compared to the BCS result [95].

For chemical potentials $\mu < 1$ GeV, the coupling constant is not small and the applicability of perturbation theory is in doubt. If we ignore this problem and extrapolate the perturbative calculation to densities $\rho \simeq 5\rho_0$ we find gaps on the order of 10's of MeV. However, perturbative estimates also show that instanton effects cannot be neglected for $\mu < 1$ GeV, and that instantons increase the gap [96].

We note that the 2SC phase defined by equ. (111) has two gapless fermions and an unbroken $SU(2)$ gauge group. The gapless fermions are singlets under the unbroken $SU(2)$. As a consequence, we expect the $SU(2)$ gauge group to become non-perturbative. An estimate of the $SU(2)$ confinement scale was given in [97]. We also note that even though the Copper pairs carry electric charge the $U(1)$ of electromagnetism is not broken. The generator of this symmetry is a linear combination of the original electric charge operator and the diagonal color charges. Under this symmetry the gapless fermions carry the charges of the proton and neutron. Possible pairing between the gapless fermions was discussed in [71,98].

5.2.2. *QCD with three flavors: Color-Flavor-Locking*

If quark matter is formed at densities several times nuclear matter density we expect the quark chemical potential to be larger than the strange quark mass. We therefore have to determine the structure of the superfluid order parameter for three quark flavors. We begin with the idealized situation of three degenerate flavors. From the arguments given in the last section we expect the order parameter to be color-flavor matrix of the form

$$\Phi^{ab}_{ij} = \langle \psi^a_i C\gamma_5 \psi^b_j \rangle. \tag{118}$$

The structure of this matrix can be determined by extremizing the grand canonical potential. We find [99,100]

$$\Delta^{ab}_{ij} = \Delta_A(\delta^a_i\delta^b_j - \delta^b_i\delta^a_j) + \Delta_S(\delta^a_i\delta^b_j + \delta^b_i\delta^a_j), \tag{119}$$

which describes the color-flavor locked (CFL) phase proposed by Alford, Rajagopal, and Wilczek [101]. In the weak coupling limit $\Delta_S \ll \Delta_A$ and $\Delta_A = 2^{-1/3}\Delta_0$ where Δ_0 is the gap in the 2SC phase, equ. (116) [99]. In the CFL phase both color and flavor symmetry are completely broken.

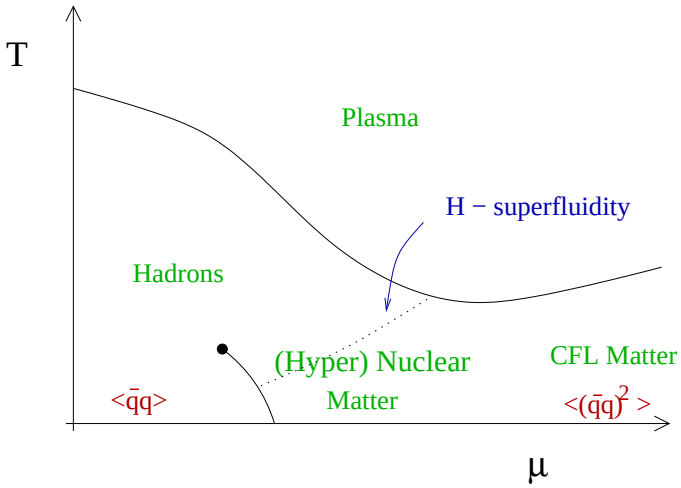

Figure 15. Conjectured phase diagram of $N_f = 3$ hadronic matter in the limit of exact flavor symmetry.

There are eight combinations of color and flavor symmetries that generate unbroken global symmetries. The unbroken symmetries are

$$\psi^a_{L,i} \to (U^*)^{ab} U_{ij} \psi^b_{Lj}, \qquad \psi^a_{R,i} \to (U^*)^{ab} U_{ij} \psi^b_{Rj}, \tag{120}$$

for $U \in SU(3)_V$. The symmetry breaking pattern is

$$SU(3)_L \times SU(3)_R \times U(1)_V \to SU(3)_V. \tag{121}$$

We observe that color-flavor-locking implies that chiral symmetry is broken. The mechanism for chiral symmetry breaking is quite unusual. The primary order parameter $\langle \psi^a_{Li} C \Delta^{ab}_{ij} \psi^b_{Lj} \rangle = -\langle \psi^a_{Ri} C \Delta^{ab}_{ij} \psi^b_{Rj} \rangle$ involves no coupling between left and right handed fermions. In the CFL phase both left and right handed flavor are locked to color, and because of the vectorial coupling of the gluon left handed flavor is effectively locked to right handed flavor. Chiral symmetry breaking also implies that $\langle \bar{\psi}\psi \rangle$ has a non-zero expectation value [102]. In the CFL phase $\langle \bar{\psi}\psi \rangle^2 \ll \langle (\bar{\psi}\psi)^2 \rangle$. Another measure of chiral symmetry breaking is provided by the pion decay constant. We will see that in the weak coupling limit f_π^2 is proportional to the density of states on the Fermi surface.

The symmetry breaking pattern $SU(3)_L \times SU(3)_R \to SU(3)_V$ in the CFL phase is identical to the symmetry breaking pattern in QCD at low density. The spectrum of excitations in the color-flavor-locked (CFL) phase

also looks remarkably like the spectrum of QCD at low density [103]. The excitations can be classified according to their quantum numbers under the unbroken $SU(3)$, and by their electric charge. The modified charge operator that generates a true symmetry of the CFL phase is given by a linear combination of the original charge operator Q_{em} and the color hypercharge operator $Q = \mathrm{diag}(-2/3, -2/3, 1/3)$. Also, baryon number is only broken modulo 2/3, which means that one can still distinguish baryons from mesons. We find that the CFL phase contains an octet of Goldstone bosons associated with chiral symmetry breaking, an octet of vector mesons, an octet and a singlet of baryons, and a singlet Goldstone boson related to superfluidity. All of these states have integer charges.

With the exception of the $U(1)$ Goldstone boson, these states exactly match the quantum numbers of the lowest lying multiplets in QCD at low density. In addition to that, the presence of the $U(1)$ Goldstone boson can also be understood. The $U(1)$ order parameter is $\langle(uds)(uds)\rangle$. This order parameter has the quantum numbers of a 0^+ $(\Lambda\Lambda)$ pair condensate. In $N_f = 3$ QCD, this is the most symmetric two nucleon channel, and a very likely candidate for superfluidity in nuclear matter at low to moderate density. We conclude that in QCD with three degenerate light flavors, there is no fundamental difference between the high and low density phases. This implies that a low density hyper-nuclear phase and the high density quark phase might be continuously connected, without an intervening phase transition. A conjectured phase diagram is shown in Fig. 15.

5.3. *The role of the strange quark mass*

At baryon densities relevant to astrophysical objects distortions of the pure CFL state due to non-zero quark masses cannot be neglected [104,105]. The most important effect of a non-zero strange quark mass is that the light and strange quark Fermi momenta will no longer be equal. When the mismatch is much smaller than the gap one calculates assuming degenerate quarks, we might expect that it has very little consequence, since at this level the original particle and hole states near the Fermi surface are mixed up anyway. On the other hand, when the mismatch is much larger than the nominal gap,we might expect that the ordering one would obtain for degenerate quarks is disrupted, and that to a first approximation one can treat the light and heavy quark dynamics separately.

This argument is qualitatively right, but the correct picture turns out to be much more complicated, and much more interesting. If the strange

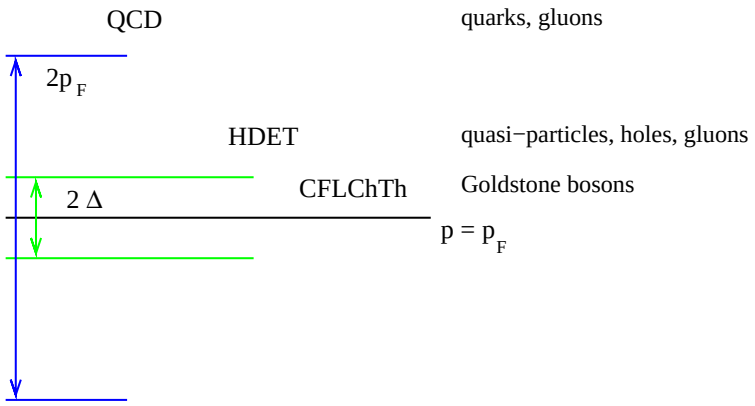

Figure 16. Hierarchy of effective field theories in the CFL phase.

quark mass is taken into account microscopic calculations based on the Dyson-Schwinger equation become much more complicated, because there are many more gap parameters, and maintaining electric neutrality and color gauge invariance is difficult [106,107,108]. However, since chiral symmetry is broken in the CFL phase we know that the dependence on the quark masses is constrained by chiral symmetry. It is therefore natural to study the problem using effective field theories. In practice we will employ a two-step procedure, see Fig. 16. In the first step we match the microscopic theory, QCD, to an effective field theory of quasi-particles and holes in the vicinity of the Fermi surface. In the second step we match this theory to an effective chiral theory for the CFL phase.

5.3.1. *High density effective theory*

The QCD Lagrangian in the presence of a chemical potential is given by

$$\mathcal{L} = \bar{\psi}\left(i\not{D} + \mu\gamma_0\right)\psi - \bar{\psi}_L M \psi_R - \bar{\psi}_R M^\dagger \psi_L - \frac{1}{4} G^a_{\mu\nu} G^a_{\mu\nu}, \qquad (122)$$

where $D_\mu = \partial_\mu + igA_\mu$ is the covariant derivative, M is the mass matrix and μ is the baryon chemical potential. If the baryon density is very large perturbative QCD calculations can be further simplified. The main observation is that the relevant degrees of freedom are particle and hole excitations in the vicinity of the Fermi surface. We shall describe these excitations in terms of the field $\psi_+(\vec{v}, x)$, where $\vec{v}$ is the Fermi velocity. At tree level, the quark field ψ can be decomposed as $\psi = \psi_+ + \psi_-$ where

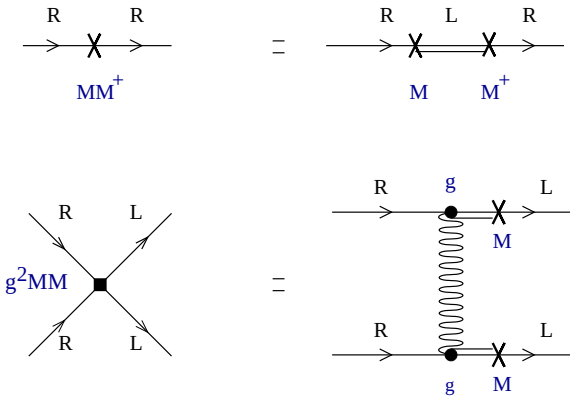

Figure 17. Mass terms in the high density effective theory. The first diagram shows a $O(MM^\dagger)$ term that arises from integrating out the ψ_- field in the QCD lagrangian. The second diagram shows a $O(M^2)$ four-fermion operator which arises from integrating out ψ_- and hard gluon exchanges.

$\psi_\pm = \frac{1}{2}(1 \pm \vec{\alpha}\cdot\hat{v})\psi$. Note that $(1 \pm \vec{\alpha}\cdot\hat{v})/2$ is a projector on states with positive/negative energy. To leading order in $1/p_F$ we can eliminate the field ψ_- using its equation of motion. The lagrangian for the ψ_+ field is given by [109,110,111]

$$\mathcal{L} = \psi_+^\dagger (iv\cdot D)\psi_+ - \frac{\Delta}{2}\left(\psi_+^{ai} C \psi_+^{bj}\,(\delta_{ai}\delta_{bj} - \delta_{aj}\delta_{bi}) + \text{h.c.}\right) + \ldots, \quad (123)$$

with $v_\mu = (1, \vec{v})$ and $i, j, \ldots$ and $a, b, \ldots$ denote flavor and color indices. The magnitude of the gap Δ is determined order by order in perturbation theory from the requirement that the thermodynamic potential is stationary with respect to Δ. With the gap term included the perturbative expansion is well defined.

The effective theory contains an infinite set of operators that have additional derivatives or more powers of ψ_+. These operators are suppressed by inverse powers of the Fermi momentum. Here, we will only consider operators that contain quark masses. To leading order in $1/p_F$ there is only one operator in the high density effective theory

$$\mathcal{L} = -\frac{1}{2p_F}\left(\psi_{L+}^\dagger M M^\dagger \psi_{L+} + \psi_{R+}^\dagger M^\dagger M \psi_{R+}\right). \quad (124)$$

This term arises from expanding the kinetic energy of a massive fermion around $p = p_F$. At $O(1/p_F^2)$ we find four-fermion operators that contain two powers of the quark mass. The coefficients of these operators are obtained by computing chirality violating quark-quark scattering amplitudes

for quasi-particles near the Fermi surface [112], see Fig. 17. At leading order in $1/p_F$ these amplitudes are independent of the scattering angle and can be represented as local four-fermion operators

$$\mathcal{L} = \frac{g^2}{8p_F^4}\left((\psi_L^{A\dagger} C\psi_L^{B\dagger})(\psi_R^C C\psi_R^D)\Gamma^{ABCD} + (\psi_L^{A\dagger}\psi_L^B)(\psi_R^{C\dagger}\psi_R^D)\tilde{\Gamma}^{ACBD}\right). \tag{125}$$

There are two additional terms with $(L \leftrightarrow R)$ and $(M \leftrightarrow M^\dagger)$. We have introduced the CFL eigenstates ψ^A defined by $\psi_i^a = \psi^A(\lambda^A)_{ai}/\sqrt{2}$, $A = 0,\ldots,8$. The tensor Γ is defined by

$$\Gamma^{ABCD} = \frac{1}{8}\Big\{\mathrm{Tr}\left[\lambda^A M(\lambda^D)^T\lambda^B M(\lambda^C)^T\right] - \frac{1}{3}\mathrm{Tr}\left[\lambda^A M(\lambda^D)^T\right]\mathrm{Tr}\left[\lambda^B M(\lambda^C)^T\right]\Big\}. \tag{126}$$

The explicit expression for $\tilde{\Gamma}$ is given in [112], but we will not need here.

5.3.2. *CFL chiral theory*

For excitation energies smaller than the gap the only relevant degrees of freedom are the Goldstone modes associated with the breaking of chiral symmetry and baryon number, see Fig. 16. Since the pattern of chiral symmetry breaking is identical to the one at $T = \mu = 0$ the effective lagrangian has the same structure as chiral perturbation theory. The main difference is that Lorentz-invariance is broken and only rotational invariance is a good symmetry. The effective lagrangian for the Goldstone modes is [113]

$$\begin{aligned}\mathcal{L}_{eff} = {} & \frac{f_\pi^2}{4}\mathrm{Tr}\left[\nabla_0\Sigma\nabla_0\Sigma^\dagger - v_\pi^2\partial_i\Sigma\partial_i\Sigma^\dagger\right] + \left[B\mathrm{Tr}(M\Sigma^\dagger) + h.c.\right] \\ & + \left[A_1\mathrm{Tr}(M\Sigma^\dagger)\mathrm{Tr}(M\Sigma^\dagger) + A_2\mathrm{Tr}(M\Sigma^\dagger M\Sigma^\dagger)\right. \\ & \left. + A_3\mathrm{Tr}(M\Sigma^\dagger)\mathrm{Tr}(M^\dagger\Sigma) + h.c.\right] + \ldots.\end{aligned} \tag{127}$$

Here $\Sigma = \exp(i\phi^a\lambda^a/f_\pi)$ is the chiral field, f_π is the pion decay constant and M is a complex mass matrix. The chiral field and the mass matrix transform as $\Sigma \to L\Sigma R^\dagger$ and $M \to LMR^\dagger$ under chiral transformations $(L,R) \in SU(3)_L \times SU(3)_R$. We have suppressed the singlet fields associated with the breaking of the exact $U(1)_V$ and approximate $U(1)_A$ symmetries.

At low density the coefficients f_π, B, $A_i,\ldots$ are non-perturbative quantities that have to extracted from experiment or measured on the lattice. At large density, on the other hand, the chiral coefficients can be calculated

in perturbative QCD. The leading order terms are [114]

$$f_\pi^2 = \frac{21 - 8\log(2)}{18}\left(\frac{p_F^2}{2\pi^2}\right), \qquad v_\pi^2 = \frac{1}{3}. \tag{128}$$

Mass terms are determined by the operators studied in the previous section. We observe that both equ. (124) and (125) are quadratic in M. This implies that $B = 0$ in perturbative QCD. B receives non-perturbative contributions from instantons, but these effects are small if the density is large [102].

We observe that $X_L = MM^\dagger/(2p_F)$ and $X_R = M^\dagger M/(2p_F)$ in equ. (124) act as effective chemical potentials for left and right-handed fermions, respectively. Formally, the effective lagrangian has an $SU(3)_L \times SU(3)_R$ gauge symmetry under which $X_{L,R}$ transform as the temporal components of non-abelian gauge fields. We can implement this approximate gauge symmetry in the CFL chiral theory by promoting time derivatives to covariant derivatives [115],

$$\nabla_0\Sigma = \partial_0\Sigma + i\left(\frac{MM^\dagger}{2p_F}\right)\Sigma - i\Sigma\left(\frac{M^\dagger M}{2p_F}\right). \tag{129}$$

The four-fermion operator in equ. (125) contributes to the coefficients A_i.We find [114,112]

$$A_1 = -A_2 = \frac{3\Delta^2}{4\pi^2}, \qquad A_3 = 0. \tag{130}$$

We can now summarize the structure of the chiral expansion in the CFL phase. The effective lagrangian has the form

$$\mathcal{L} \sim f_\pi^2\Delta^2\left(\frac{\partial_0}{\Delta}\right)^k\left(\frac{\vec{\partial}}{\Delta}\right)^l\left(\frac{MM^\dagger}{p_F\Delta}\right)^m\left(\frac{MM}{p_F^2}\right)^n(\Sigma)^o(\Sigma^\dagger)^p. \tag{131}$$

Loop graphs in the effective theory are suppressed by powers of $\partial/(4\pi f_\pi)$. Since the pion decay constant scales as $f_\pi \sim p_F$ Goldstone boson loops are suppressed compared to higher order contact terms. We also note that the quark mass expansion is controlled by $m^2/(p_F\Delta)$, as expected from the arguments presented in Sect. 5.3.

5.3.3. *Kaon condensation*

Using the chiral effective lagrangian we can now determine the dependence of the order parameter on the quark masses. We will focus on the physically relevant case $m_s > m_u = m_d$. Because the main expansion parameter is

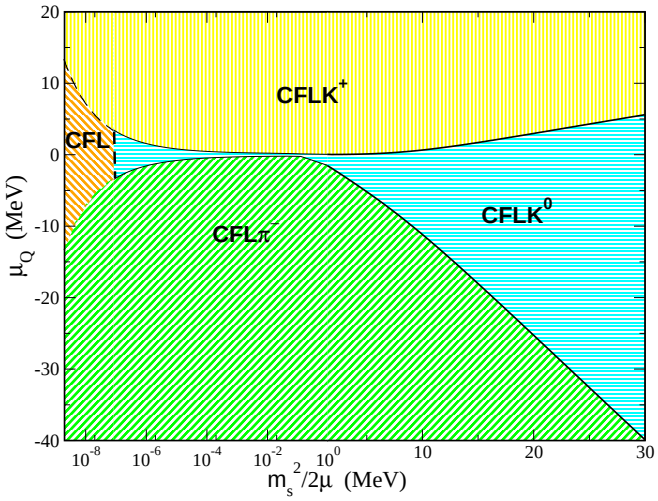

Figure 18. This figure shows the phase structure of CFL matter as a function of the strange quark mass m_s and the lepton chemical potential μ_Q, from Kaplan and Reddy (2001).

$m_s^2/(p_F\Delta)$ increasing the quark mass is roughly equivalent to lowering the density. The effective potential for the order parameter is

$$V_{eff} = \frac{f_\pi^2}{2}\mathrm{Tr}\left[X_L\Sigma X_R\Sigma^\dagger\right] + A_1\left[\left(\mathrm{Tr}(M\Sigma^\dagger)\right)^2 - \mathrm{Tr}(M\Sigma^\dagger M\Sigma^\dagger)\right]. \quad (132)$$

If the strange quark mass is small then the minimum of the effective potential is $\Sigma = 1$. However, when the strange quark mass exceeds a certain critical value it becomes favorable to rotate the order parameter in the kaon direction. The physical reason is that the system tries to reduce its strangeness content by forming a kaon condensate. Consider the ansatz $\Sigma = \exp(i\alpha\lambda_4)$. The vacuum energy is

$$V(\alpha) = -f_\pi^2\left(\frac{1}{2}\left(\frac{m_s^2 - m^2}{2p_F}\right)^2\sin(\alpha)^2 + (m_K^0)^2(\cos(\alpha) - 1)\right), \quad (133)$$

where $(m_K^0)^2 = (4A_1/f_\pi^2)m(m + m_s)$. Minimizing the vacuum energy we obtain $\alpha = 0$ if $\mu_s < m_K^0$ and $\cos(\alpha) = (m_K^0)^2/\mu_s^2$ if $\mu_s > m_K^0$. Here, we have defined $\mu_s = m_s^2/(2p_F)$. Using the perturbative result for A_1 the

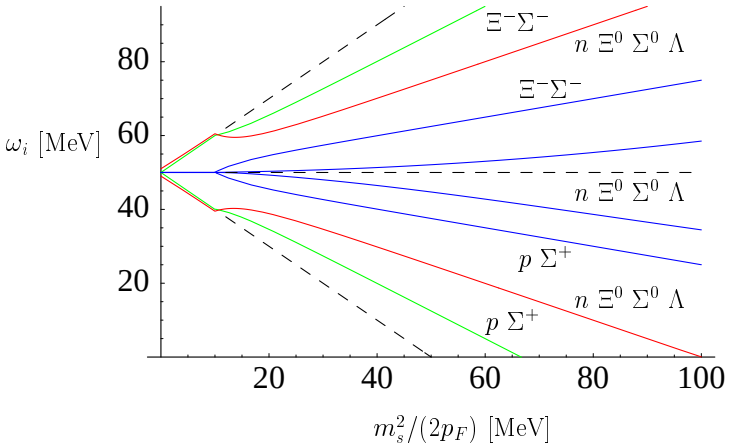

Figure 19. This figure shows the fermion spectrum in the CFL phase. For $m_s = 0$ there are eight fermions with gap Δ and one fermion with gap 2Δ (not shown). Without kaon condensation gapless fermion modes appear at $\mu_s = \Delta$ (dashed lines). With kaon condensation gapless modes appear at $\mu_s = 4\Delta/3$.

critical strange quark mass is

$$m_s|_{crit} = 3.03 \cdot m_d^{1/3} \Delta^{2/3}. \tag{134}$$

Using $\Delta \simeq 50$ MeV we get $m_s(crit) \simeq 70$ MeV. This result suggests that strange quark matter at densities $\rho \sim (5-10)\rho_0$ is in a kaon condensed phase. The kaon condensate breaks $SU(2)_I \times U(1)_Y$ to $U(1)_Q$. The phase structure as a function of the strange quark mass and non-zero lepton chemical potentials was studied by Kaplan and Reddy [116], see Fig. 18. We observe that if the lepton chemical potential is non-zero charged kaon and pion condensates are also possible. It was also shown that there is a range of light quark masses in which simultaneous kaon and eta condensation takes place [117].

6. Fermions in the CFL phase

So far we have only studied Goldstone modes in the CFL phase. However, as the strange quark mass is increased it is possible that some of the fermion modes become light or even gapless [118]. In order to study this question we have to include fermions in the effective field theory. The effective

lagrangian for fermions in the CFL phase is [119,120]

$$\mathcal{L} = \mathrm{Tr}\left(N^\dagger i v^\mu D_\mu N\right) - D\mathrm{Tr}\left(N^\dagger v^\mu \gamma_5 \{\mathcal{A}_\mu, N\}\right) - F\mathrm{Tr}\left(N^\dagger v^\mu \gamma_5 [\mathcal{A}_\mu, N]\right) + \frac{\Delta}{2}\left\{\left(\mathrm{Tr}\left(N_L N_L\right) - \left[\mathrm{Tr}\left(N_L\right)\right]^2\right) - (L \leftrightarrow R) + h.c.\right\}. \quad (135)$$

$N_{L,R}$ are left and right handed baryon fields in the adjoint representation of flavor $SU(3)$. The baryon fields originate from quark-hadron complementarity as explained in Sect. 5.2.2. We can think of N as being composed of a quark and a diquark field, $N_L \sim q_L \langle q_L q_L \rangle$. The covariant derivative of the nucleon field is given by $D_\mu N = \partial_\mu N + i[\mathcal{V}_\mu, N]$. The vector and axial-vector currents are

$$\mathcal{V}_\mu = -\frac{i}{2}\left\{\xi \partial_\mu \xi^\dagger + \xi^\dagger \partial_\mu \xi\right\}, \qquad \mathcal{A}_\mu = -\frac{i}{2}\xi\left(\nabla_\mu \Sigma^\dagger\right)\xi, \quad (136)$$

where ξ is defined by $\xi^2 = \Sigma$. It follows that ξ transforms as $\xi \to L\xi U(x)^\dagger = U(x)\xi R^\dagger$ with $U(x) \in SU(3)_V$. For pure $SU(3)$ flavor transformations $L = R = V$ we have $U(x) = V$. F and D are low energy constants that determine the baryon axial coupling. In perturbative QCD we find $D = F = 1/2$.

Mass terms can be introduced as in Sect. 5.3.2. The (X_L, X_R) covariant derivative of the nucleon field is

$$D_0 N = \partial_0 N + i[\Gamma_0, N], \quad (137)$$
$$\Gamma_0 = -\frac{i}{2}\left\{\xi\left(\partial_0 + iX_R\right)\xi^\dagger + \xi^\dagger\left(\partial_0 + iX_L\right)\xi\right\},$$

where $X_L = MM^\dagger/(2p_F)$ and $X_R = M^\dagger M/(2p_F)$ as before. The spectrum of fermion is shown in Fig. 19. A gapless fermion mode appears at $\mu_s = 4\Delta/3$. In the vicinity of this point the homogeneous CFL phase becomes unstable [121,122]. In the effective field theory this manifests itself as an instability with respect to the generation of a non-zero current [123,124]. From the effective lagrangian equ. (127) we see that a meson current has energy $\mathcal{E} \sim f_\pi^2 j^2$. This is not the end of the story, however, because a meson current also modifies the fermion dispersion relation. The energy of the lowest mode in the background of a hypercharge current j_K is given by

$$\omega_l = \Delta + \frac{l^2}{2\Delta} - \frac{3}{4}\mu_s - \frac{1}{4}\vec{v}\cdot\vec{j}_K, \quad (138)$$

where l is the momentum relative to the Fermi surface. We observe that the current lowers the energy of the fermions on part of the Fermi surface. When these states become gapless the total energy is lowered and

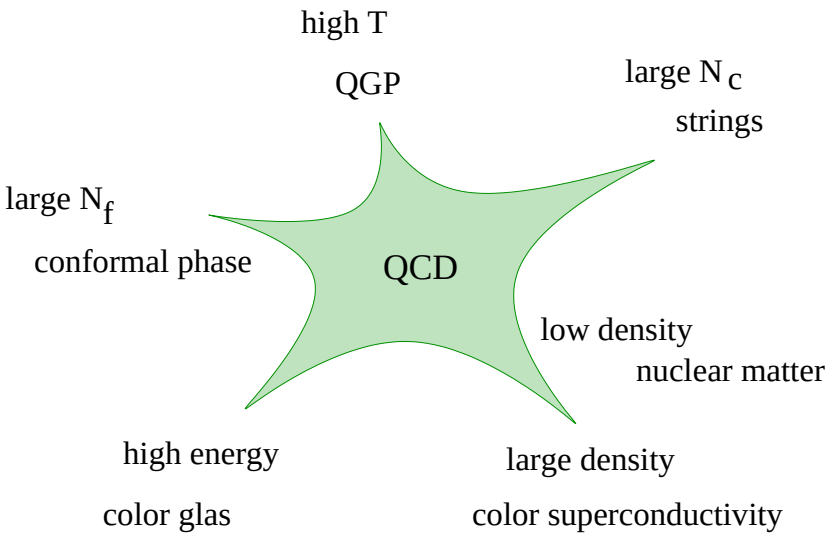

Figure 20. The many facets of QCD.

the system can become unstable. The new ground state is a p-wave meson condensate in which the non-zero meson current is balanced by a back-flow of gapless fermions. At even larger values of μ_s this state may evolve into an inhomogeneous superconductor of the type considered by Larkin, Ovchinnikov, Fulde and Ferrell [125,126], see [127].

7. Outlook

Figure 20 indicates that there are many interesting connections that we have not been able to explore in these lectures. There has been a lot of progress in connecting the large N_c world to a theory of strings, and this connection also sheds some light on the behavior of a strongly coupled QCD plasma. The transport properties of the strongly coupled plasma are probably quite similar to the transport behavior of the strongly correlated neutron fluid, and this system is related to cold trapped fermionic atoms near a Feshbach resonance. A lot of progress has been made in understanding hot and dense pre-equilibrium states, and these states share some of the properties of equilibrium phases. Many more surprising connections are likely to energy in the future.

Acknowledgments: I would like to thank the organizers of the HUGS summer school, especially Jose Goity, for their hospitality. The original lec-

tures contained a summary of the experimental work at RHIC and CERN. This material is not included in the write-up, but the slides are still available on my website. The second half of the lectures is an abridged and updated version of the NPSS lectures [11]. Fig. 20 was inspired by R. Brower. This work was supported in part by a US DOE grant DE-FG-88ER40388.

References

1. E. V. Shuryak, The QCD vacuum, hadrons, and the superdense matter, World Scientific, Singapore (1988).
2. J. B. Kogut and M. A. Stephanov, Camb. Monogr. Part. Phys. Nucl. Phys. Cosmol. **21**, 1 (2004).
3. D. H. Rischke, Prog. Part. Nucl. Phys. **52**, 197 (2004) [nucl-th/0305030].
4. J. Kapusta, Finite temperature field theory, Cambridge University Press, Cambridge (1989).
5. M. LeBellac, Thermal Field Theory, Cambridge University Press, Cambridge (1996).
6. U. Kraemmer and A. Rebhan, Rept. Prog. Phys. **67**, 351 (2004) [hep-ph/0310337].
7. A. L. Fetter and J. D. Walecka, Quantum theory of many particle systems, McGraw Hill, New York (1971).
8. A. A. Abrikosov, L. P. Gorkov and I. E. Dzyaloshinski, Methods of quantum field theory in statistical physics, Prentice-Hall, Englewood Cliffs, N.J. (1963).
9. K. Rajagopal and F. Wilczek, The condensed matter physics of QCD, in: Festschrift in honor of B.L. Ioffe, 'At the Frontier of Particle Physics / Handbook of QCD', M. Shifman, ed., World Scientific, Singapore, hep-ph/0011333.
10. M. G. Alford, Ann. Rev. Nucl. Part. Sci. **51**, 131 (2001) [hep-ph/0102047].
11. T. Schäfer, "Quark matter", in "Quarks and Mesons", A. B. Santra et.al, Eds., Narosa Publishing House, New Dehli (2004) [hep-ph/0304281].
12. M. Buballa, Phys. Rept. **407**, 205 (2005) [hep-ph/0402234].
13. H. C. Ren, preprint, hep-ph/0404074.
14. M. Huang, Int. J. Mod. Phys. E **14**, 675 (2005) [hep-ph/0409167].
15. I. A. Shovkovy, preprint, nucl-th/0410091.
16. I. Arsenne et al. [Brahms], B. Back et al. [Phobos], K. Adcox et al. [Phenix], J. Adams et al. [Star], "First Three Years of Operation of RHIC", Nucl. Phys. **A757**, 1-183 (2005).
17. G. Nardulli, Riv. Nuovo Cim. **25N3**, 1 (2002) [hep-ph/0202037].
18. S. Reddy, Acta Phys. Polon. B **33**, 4101 (2002) [nucl-th/0211045].
19. D. J. Gross and F. Wilczek, Phys. Rev. Lett. **30**, 1343 (1973).
20. H. D. Politzer, Phys. Rev. Lett. **30**, 1346 (1973).
21. S. Elitzur, Phys. Rev. D **12**, 3978 (1975).
22. C. Vafa and E. Witten, Nucl. Phys. B **234**, 173 (1984).
23. C. Vafa and E. Witten, Phys. Rev. Lett. **53**, 535 (1984).
24. R. F. Dashen, Phys. Rev. D **3**, 1879 (1971).

25. K. A. Intriligator and N. Seiberg, Nucl. Phys. Proc. Suppl. **45BC**, 1 (1996) [hep-th/9509066].
26. T. Banks and A. Zaks, Nucl. Phys. B **196**, 189 (1982).
27. G. 't Hooft, in: Recent developments in gauge theories, G. 't Hooft, editor, Plenum Press, New York (1980).
28. M. Peskin, in: Recent advances in field theory and statistical mechanics, Les Houches 1982, J. B. Zuber and R. Stora, editors, North Holland, Amsterdam (1984).
29. S. R. Coleman and E. Witten, Phys. Rev. Lett. **45**, 100 (1980).
30. I. I. Kogan, A. Kovner and M. A. Shifman, Phys. Rev. D **59**, 016001 (1999) [hep-ph/9807286].
31. J. C. Collins and M. J. Perry, Phys. Rev. Lett. **34**, 1353 (1975).
32. E. V. Shuryak, Sov. Phys. JETP **47**, 212 (1978) [Zh. Eksp. Teor. Fiz. **74**, 408 (1978)].
33. E. V. Shuryak, Phys. Lett. B **78**, 150 (1978) [Sov. J. Nucl. Phys. **28**, 408 (1978)].
34. M. A. Shifman, A. I. Vainshtein and V. I. Zakharov, Nucl. Phys. B **147**, 385 (1979).
35. J. Gasser and H. Leutwyler, Phys. Lett. B **184**, 83 (1987).
36. D. J. Gross, R. D. Pisarski and L. G. Yaffe, Rev. Mod. Phys. **53**, 43 (1981).
37. M. Creutz, Quarks, Gluons And Lattices, Cambridge University Press (1984).
38. B. Svetitsky and L. G. Yaffe, Nucl. Phys. B **210**, 423 (1982).
39. S. Digal, E. Laermann and H. Satz, Eur. Phys. J. C **18**, 583 (2001) [hep-ph/0007175].
40. A. Mocsy, F. Sannino and K. Tuominen, Phys. Rev. Lett. **92**, 182302 (2004) [hep-ph/0308135].
41. C. Ratti, M. A. Thaler and W. Weise, preprint, hep-ph/0506234.
42. S. Chandrasekharan and U. J. Wiese, Prog. Part. Nucl. Phys. **53**, 373 (2004) [hep-lat/0405024].
43. E. Laermann and O. Philipsen, Ann. Rev. Nucl. Part. Sci. **53**, 163 (2003) [hep-ph/0303042].
44. E. Braaten and R. D. Pisarski, Nucl. Phys. B **337**, 569 (1990).
45. Z. Fodor and S. D. Katz, JHEP **0203**, 014 (2002) [hep-lat/0106002].
46. P. de Forcrand and O. Philipsen, Nucl. Phys. B **642**, 290 (2002) [hep-lat/0205016].
47. C. R. Allton *et al.*, Phys. Rev. D **66**, 074507 (2002) [hep-lat/0204010].
48. H. W. Hammer and R. J. Furnstahl, Nucl. Phys. A **678**, 277 (2000) [nucl-th/0004043].
49. T. D. Lee and C. N. Yang, Phys. Rev. **105**, 1119 (1957).
50. K. Huang and C. N. Yang, Phys. Rev. **105**, 767 (1957).
51. J. Kinast, A. Turlapov, J. E. Thomas, Q. Chen, J. Stajic, K. Levin Science, 27 January 2005 (10.1126/science.1109220) [cond-mat/0502087].
52. T. Schäfer, C. W. Kao and S. R. Cotanch, preprint, nucl-th/0504088.
53. J. V. Steele, preprint, nucl-th/0010066.
54. J. Carlson, J. J. Morales, V. R. Pandharipande and D. G. Ravenhall, Phys. Rev. C **68**, 025802 (2003) [nucl-th/0302041].

55. J. W. Chen and D. B. Kaplan, Phys. Rev. Lett. **92**, 257002 (2004) [hep-lat/0308016].
56. M. Wingate, preprint, hep-lat/0409060.
57. D. Lee and T. Schäfer, preprint, nucl-th/0412002.
58. A. Bulgac, J. E. Drut and P. Magierski, preprint, cond-mat/0505374.
59. R. Shankar, Rev. Mod. Phys. **66**, 129 (1994).
60. J. Polchinski, Effective field theory and the Fermi surface, Lectures presented at TASI 92, Boulder, CO, hep-th/9210046.
61. T. Papenbrock and G. F. Bertsch, Phys. Rev. C **59**, 2052 (1999) [nucl-th/9811077].
62. V. A. Khodel, V. V. Khodel, and J. W. Clark, Nucl. Phys. A**598** (1996) 390.
63. L. P. Gorkov and T. K. Melik-Barkhudarov, Sov. Phys. JETP **13**, 1018 (1961).
64. J. Carlson, S.-Y. Chang, V. R. Pandharipande, and K. E. Schmidt, Phys. Rev. Lett. **91**, 050401, (2003).
65. P. W. Anderson, Basic notions of condensed matter physics, Benjamin/Cummings Pub. Co., Menlo Park, CA (1984).
66. S. Weinberg, The quantum theory of fields, vol. II, Cambridge University Press (1995).
67. S. C. Frautschi, Asymptotic freedom and color superconductivity in dense quark matter, in: Proceedings of the Workshop on Hadronic Matter at Extreme Energy Density, N. Cabibbo, Editor, Erice, Italy (1978).
68. B. C. Barrois, Nucl. Phys. **B129**, 390 (1977).
69. F. Barrois, Nonperturbative effects in dense quark matter, Ph.D. thesis, Caltech, UMI 79-04847-mc (microfiche).
70. D. Bailin and A. Love, Phys. Rept. **107**, 325 (1984).
71. M. Alford, K. Rajagopal and F. Wilczek, Phys. Lett. **B422**, 247 (1998) [hep-ph/9711395].
72. R. Rapp, T. Schäfer, E. V. Shuryak and M. Velkovsky, Phys. Rev. Lett. **81**, 53 (1998) [hep-ph/9711396].
73. R. D. Pisarski and F. Wilczek, Phys. Rev. D **29**, 338 (1984).
74. A. Barducci, R. Casalbuoni, S. De Curtis, R. Gatto and G. Pettini, Phys. Lett. B **231**, 463 (1989).
75. J. Berges and K. Rajagopal, Nucl. Phys. B **538**, 215 (1999) [hep-ph/9804233].
76. M. A. Halasz, A. D. Jackson, R. E. Shrock, M. A. Stephanov and J. J. Verbaarschot, Phys. Rev. D **58**, 096007 (1998) [hep-ph/9804290].
77. M. Stephanov, K. Rajagopal and E. V. Shuryak, Phys. Rev. Lett. **81**, 4816 (1998) [hep-ph/9806219].
78. M. Kitazawa, T. Koide, T. Kunihiro and Y. Nemoto, Prog. Theor. Phys. **108**, 929 (2002) [hep-ph/0207255].
79. N. Evans, S. D. Hsu and M. Schwetz, Nucl. Phys. **B551**, 275 (1999) [hep-ph/9808444].
80. T. Schäfer and F. Wilczek, Phys. Lett. **B450**, 325 (1999) [hep-ph/9810509].
81. W. E. Brown, J. T. Liu and H. C. Ren, Phys. Rev. D **62**, 054016 (2000) [hep-ph/9912409].
82. T. Schäfer, Phys. Rev. **D62**, 094007 (2000) [hep-ph/0006034].

83. D. T. Son, Phys. Rev. **D59**, 094019 (1999) [hep-ph/9812287].
84. T. Schäfer and F. Wilczek, Phys. Rev. **D60**, 114033 (1999) [hep-ph/9906512].
85. R. D. Pisarski and D. H. Rischke, Phys. Rev. **D61**, 074017 (2000) [nucl-th/9910056].
86. D. K. Hong, V. A. Miransky, I. A. Shovkovy and L. C. Wijewardhana, Phys. Rev. **D61**, 056001 (2000) [hep-ph/9906478].
87. W. E. Brown, J. T. Liu and H. c. Ren, Phys. Rev. D **61**, 114012 (2000) [hep-ph/9908248].
88. C. Manuel, Phys. Rev. D **53**, 5866 (1996) [hep-ph/9512365].
89. W. E. Brown, J. T. Liu and H. c. Ren, Phys. Rev. D **62**, 054013 (2000) [hep-ph/0003199].
90. A. Ipp, A. Gerhold and A. Rebhan, Phys. Rev. D **69**, 011901 (2004) [hep-ph/0309019].
91. T. Schäfer and K. Schwenzer, Phys. Rev. D **70**, 054007 (2004) [hep-ph/0405053].
92. Q. Wang and D. H. Rischke, Phys. Rev. D **65**, 054005 (2002) [nucl-th/0110016].
93. T. Schäfer, Nucl. Phys. A **728**, 251 (2003) [hep-ph/0307074].
94. T. Matsuura, K. Iida, T. Hatsuda and G. Baym, Phys. Rev. D **69**, 074012 (2004) [hep-ph/0312042].
95. I. Giannakis, D. f. Hou, H. c. Ren and D. H. Rischke, Phys. Rev. Lett. **93**, 232301 (2004) [hep-ph/0406031].
96. T. Schäfer, Proceedings of KIAS-APCTP International Symposium in Astro-Hadron Physics: Compact Stars: Quest for New States of Dense Matter, Seoul, Korea, World Scientific, Singapore (2005) [hep-ph/0402032].
97. D. H. Rischke, D. T. Son and M. A. Stephanov, Phys. Rev. Lett. **87**, 062001 (2001) [hep-ph/0011379].
98. M. G. Alford, J. A. Bowers, J. M. Cheyne and G. A. Cowan, Phys. Rev. D **67**, 054018 (2003) [hep-ph/0210106].
99. T. Schäfer, Nucl. Phys. B **575**, 269 (2000) [hep-ph/9909574].
100. N. Evans, J. Hormuzdiar, S. D. Hsu and M. Schwetz, Nucl. Phys. B **581**, 391 (2000) [hep-ph/9910313].
101. M. Alford, K. Rajagopal and F. Wilczek, Nucl. Phys. **B537**, 443 (1999) [hep-ph/9804403].
102. T. Schäfer, Phys. Rev. D **65**, 094033 (2002) [hep-ph/0201189].
103. T. Schäfer and F. Wilczek, Phys. Rev. Lett. **82**, 3956 (1999) [hep-ph/9811473].
104. M. Alford, J. Berges and K. Rajagopal, Nucl. Phys. **B558**, 219 (1999) [hep-ph/9903502].
105. T. Schäfer and F. Wilczek, Phys. Rev. **D60**, 074014 (1999) [hep-ph/9903503].
106. A. W. Steiner, S. Reddy and M. Prakash, Phys. Rev. D **66**, 094007 (2002) [hep-ph/0205201].
107. M. Alford and K. Rajagopal, JHEP **0206**, 031 (2002) [hep-ph/0204001].
108. F. Neumann, M. Buballa and M. Oertel, Nucl. Phys. A **714**, 481 (2003) [hep-ph/0210078].

109. D. K. Hong, Phys. Lett. B **473**, 118 (2000) [hep-ph/981251].
110. D. K. Hong, Nucl. Phys. B **582**, 451 (2000) [hep-ph/9905523].
111. S. R. Beane, P. F. Bedaque and M. J. Savage, Phys. Lett. B **483**, 131 (2000) [hep-ph/0002209].
112. T. Schäfer, Phys. Rev. D **65**, 074006 (2002) [hep-ph/0109052].
113. R. Casalbuoni and D. Gatto, Phys. Lett. **B464**, 111 (1999) [hep-ph/9908227].
114. D. T. Son and M. Stephanov, Phys. Rev. **D61**, 074012 (2000) [hep-ph/9910491], erratum: hep-ph/0004095.
115. P. F. Bedaque and T. Schäfer, Nucl. Phys. **A697**, 802 (2002) [hep-ph/0105150].
116. D. B. Kaplan and S. Reddy, Phys. Rev. D **65**, 054042 (2002) [hep-ph/0107265].
117. A. Kryjevski, D. B. Kaplan and T. Schäfer, Phys. Rev. D **71**, 034004 (2005) [hep-ph/0404290].
118. M. Alford, C. Kouvaris and K. Rajagopal, Phys. Rev. Lett. **92**, 222001 (2004) [hep-ph/0311286].
119. A. Kryjevski and T. Schäfer, Phys. Lett. B **606**, 52 (2005) [hep-ph/0407329].
120. A. Kryjevski and D. Yamada, Phys. Rev. D **71**, 014011 (2005) [hep-ph/0407350].
121. M. Huang and I. A. Shovkovy, Phys. Rev. D **70**, 051501 (2004) [hep-ph/0407049].
122. R. Casalbuoni, R. Gatto, M. Mannarelli, G. Nardulli and M. Ruggieri, Phys. Lett. B **605**, 362 (2005) [hep-ph/0410401].
123. A. Kryjevski, preprint, hep-ph/0508180.
124. T. Schäfer, preprint, hep-ph/0508190.
125. A. I. Larkin and Yu. N. Ovchinikov, Zh. Eksp. Theor. Fiz. **47**, 1136 (1964); engl. translation: Sov. Phys. JETP **20**, 762 (1965).
126. P. Fulde and A. Ferrell, Phys. Rev. **145**, A550 (1964).
127. R. Casalbuoni, R. Gatto, N. Ippolito, G. Nardulli and M. Ruggieri, preprint, hep-ph/0507247.